PROBLEM-PARAMETER FREE FEDERATED LEARNING

Anonymous authors
Paper under double-blind review

ABSTRACT

Federated learning (FL) has garnered significant attention from academia and industry in recent years due to its advantages in data privacy, scalability, and communication efficiency. However, current FL algorithms face a critical limitation: their performance heavily depends on meticulously tuned hyperparameters, particularly the learning rate or stepsize. This manual tuning process is challenging in federated settings due to data heterogeneity and limited accessibility of local datasets. Consequently, the reliance on problem-specific parameters hinders the widespread adoption of FL and potentially compromises its performance in dynamic or diverse environments. To address this issue, we introduce PAdaMFed, a novel algorithm for nonconvex FL that carefully combines adaptive stepsize and momentum techniques. PAdaMFed offers two key advantages: 1) it operates autonomously without relying on problem-specific parameters, making it, to our knowledge, the first FL algorithm to achieve such problem-parameter-agnostic adaptation; and 2) it manages data heterogeneity and partial participation without requiring heterogeneity bounds. Despite these benefits, PAdaMFed provides several strong theoretical guarantees: 1) It achieves state-of-the-art convergence rates with a sample complexity of $\mathcal{O}(\epsilon^{-4})$ and communication complexity of $\mathcal{O}(\epsilon^{-3})$ to obtain an accuracy of $\|\nabla f(\boldsymbol{\theta})\| \leq \epsilon$, even using constant learning rates; 2) these complexities can be improved to the best-known $\mathcal{O}(\epsilon^{-3})$ for sampling and $\mathcal{O}(\epsilon^{-2})$ for communication when incorporating variance reduction; 3) it exhibits linear speedup with respect to the number of local update steps and participating clients at each global round. These attributes make PAdaMFed highly scalable and adaptable for various real-world FL applications. Extensive empirical evidence on both image classification and sentiment analysis tasks validates the efficacy of our approaches.

1 INTRODUCTION

Federated learning (FL) has emerged as a promising paradigm for machine learning, allowing multiple clients to collaboratively train a model without sharing raw data. Since its introduction by McMahan et al. (2017), FL has garnered substantial attention from both academia and industry. Major conferences such as NeurIPS, ICML, and ICLR have witnessed a proliferation of FL-related research, addressing critical challenges including communication efficiency (Chen et al., 2021; Sattler et al., 2019), privacy preservation (Wei et al., 2020; Mothukuri et al., 2021), heterogeneity management Li et al. (2020); Karimireddy et al. (2020b); Wang et al. (2020), and partial and asynchronous participation (Wang et al., 2024; Xu et al., 2023).

Despite significant advancements, current FL algorithms face a critical limitation: their performance heavily depends on meticulously tuned hyperparameters, particularly the learning rate or stepsize. This tuning process typically requires extensive computational resources and problem-specific knowledge, such as smoothness parameters, heterogeneity bounds, stochastic gradient variances, and initial optimality gaps. For instance, MIME (Karimireddy et al., 2020a) relies on smoothness constants and data heterogeneity bounds for stepsize determination, FedProx (Li et al., 2020) requires careful adjustment of a proximal term based on data heterogeneity, and FedDyn (Acar et al., 2021) demands tuning of a regularization parameter contingent on problem characteristics. Furthermore, algorithms such as FedADT (Gao et al., 2023) and FedAMS (Chen et al., 2020) necessitate problem-specific parameters to establish minimum communication rounds, which must exceed thresholds associated with smoothness and other hyperparameters.

This reliance on problem-specific parameters poses several critical challenges. First, it impedes the widespread adoption of FL by complicating deployment and requiring expertise for hyperparameter tuning (Mostafa, 2019; Deng et al., 2020). Second, it potentially compromises performance in dynamic or diverse environments where data distributions may evolve (Reddi et al., 2020; Koloskova et al., 2020). Last, accurately estimating these parameters in federated settings is often infeasible due to the distributed nature of data and the inherent privacy constraints of FL (Konečnỳ et al., 2016).

Recent research has attempted to address this issue through adaptive stepsize methods. FedOpt (Reddi et al., 2020) incorporates adaptive optimization techniques like AdaGrad, Adam, and Yogi into FL, demonstrating improved convergence compared to FedAvg (McMahan et al., 2017). FedNova (Wang et al., 2020) introduces a normalization technique that effectively mitigates objective inconsistency caused by partial client participation and data heterogeneity. FedBN (Li et al., 2021) employed local batch normalization to alleviate feature shift before averaging models, outperforming both classical FedAvg (McMahan et al., 2017) and FedProx (Li et al., 2020) for non-IID data. While these approaches show promise, they still require careful tuning of global learning rates.

Momentum is a technique that mitigates data heterogeneity and accelerates gradient descent by maintaining a velocity vector of gradient history. Recent studies have investigated the combination of adaptive methods with momentum to leverage both advantages. Hsu et al. (2019) proposed FedAvgM, which incorporates a server-side momentum term into the FedAvg algorithm, demonstrating enhanced convergence rates and robustness against data heterogeneity. Wang et al. (2019) developed SlowMo, a momentum-based method that employs two nested loops to facilitate faster convergence in distributed optimization. FedAMS (Chen et al., 2020) utilizes adaptive moment methods on both the server and client sides to address data heterogeneity. MIME (Karimireddy et al., 2020a) combines client and server momentum to enhance convergence. Wu et al. (2023) introduced FAFED, a momentum-based variance reduction scheme integrated with an adaptive matrix, achieving the best-known sample and communication complexity when utilizing diminishing stepsizes. Nevertheless, these methods still necessitate fine-tuning of multiple hyperparameters, limiting their practical applicability.

A very recent contribution, FedSPS (Sohom Mukherjee, 2024), claims to be the first fully locally adaptive method for FL with minimal hyperparameter tuning. While promising, this approach relies on stringent assumptions of bounded gradients and bounded data heterogeneity. Moreover, it fails to converge to optima with constant stepsizes and requires adjustment of a maximum stepsize threshold based on the smoothness parameter, maintaining a degree of hyperparameter dependence. Therefore, there is a critical need for more robust and adaptive FL algorithms capable of operating effectively across diverse scenarios without relying on problem-specific parameters.

1.1 Main Contributions

This paper addresses these critical limitations of FL by proposing a novel approach that eliminates the need for problem-specific parameters while effectively handling arbitrary heterogeneous data and supporting partial client participation. Our method is based on a careful combination of adaptive stepsize and momentum techniques. The adaptive stepsize mechanism dynamically adjusts local learning rates against client update heterogeneity, while the momentum component provides stability under partial participation and accelerates convergence in the nonconvex landscape. Our main contributions are summarized below.

1) We introduce PAdaMFed, a problem-specific **P**arameter **A**gnostic algorithm for nonconvex FL based on **ada**ptive stepsizes and client-side **M**omentum. PAdaMFed offers several significant advantages:
   - *Independent of problem-specific parameters:* PAdaMFed operates autonomously without relying on any problem-specific parameters such as smoothness constants or stochastic gradient variance. All stepsizes in our approach are explicitly determined by the number of participating clients, local updates, and communication rounds. To the best of our knowledge, this is the first algorithm to achieve such parameter-agnostic adaptation in FL.
   - *Robustness to arbitrary heterogeneous data:* PAdaMFed inherently manages data heterogeneity without requiring any heterogeneity bounds among clients while accommodating partial client participation. This feature enhances its scalability and adaptability in real-world scenarios where client data can be highly diverse and unpredictable, and full participation may not always be feasible due to resource constraints or device availability.

2) We provide a rigorous theoretical analysis of PAdaMFed, demonstrating its state-of-the-art performance:
   - PAdaMFed achieves a sample complexity of $\mathcal{O}(\epsilon^{-4})$ and communication complexity of $\mathcal{O}(\epsilon^{-3})$ to obtain a $\|\nabla f(\boldsymbol{\theta})\| \leq \epsilon$ accuracy for nonconvex FL problems, even using constant learning rates.
   - The complexities are further improved to the best-known sample complexity of $\mathcal{O}(\epsilon^{-3})$ and communication complexity of $\mathcal{O}(\epsilon^{-2})$ when incorporating variance reduction.
   - PAdaMFed exhibits linear speedup with respect to the numbers of local update steps and participating clients in each global round.

   Notably, these theoretical results are obtained under minimal assumptions, requiring only L-smoothness of loss functions and unbiased stochastic gradients with bounded within-client variance. This represents a significant advancement over existing FL algorithms, which typically necessitate constraints such as data heterogeneity bounds (Li et al., 2021; Wu et al., 2023), diminishing stepsizes (Wu et al., 2023; Sohom Mukherjee, 2024), or fail to achieve the best-known convergence rates (Liang et al., 2019; Alghunaim, 2024).
3) We conduct empirical evaluations on both image classification and sentiment analysis tasks to validate our theoretical findings and the efficacy of our algorithms. Our methods are compared against several established baselines, including FedAvg (McMahan et al., 2017), SCAFFOLD (Karimireddy et al., 2020b), and SCAFFOLD-M (Cheng et al., 2024). Extensive numerical evidence demonstrates the superiority of our approaches in not only stepsize robustness but also testing accuracy and convergence speed.

2 Problem Setup

We consider an FL system where N clients collaboratively train a common learning model $\boldsymbol{\theta} \in \mathbb{R}^d$ under the coordination of a parameter server. Let $\boldsymbol{\xi}_i$ represent a random sample of client i drawn from its local data distribution $\mathcal{D}_i$. The loss function associated with client i is given by $f_i(\boldsymbol{\theta}) := \mathbb{E}_{\boldsymbol{\xi}_i \sim \mathcal{D}_i}[F(\boldsymbol{\theta}; \boldsymbol{\xi}_i)]$, where $F(\boldsymbol{\theta}; \boldsymbol{\xi}_i)$ is the stochastic loss of client i over sample $\boldsymbol{\xi}_i$. The objective of the FL system is to minimize the global loss function across all clients, defined as:

$$\min_{\boldsymbol{\theta} \in \mathbb{R}^d} f(\boldsymbol{\theta}) := \frac{1}{N} \sum_{i=1}^{N} f_i(\boldsymbol{\theta}) \quad \text{where} \quad f_i(\boldsymbol{\theta}) := \mathbb{E}_{\boldsymbol{\xi}_i \sim \mathcal{D}_i}[F(\boldsymbol{\theta}; \boldsymbol{\xi}_i)].$$

In a federated setting, clients collaboratively train a global model, but the raw data of each client is never shared with the server and other clients.

Denote by $\|\cdot\|$ the ℓ_2 norm. We make the following assumptions.

Assumption 1 (Sample-Wise Smoothness)**.** *Given any $\boldsymbol{\xi}$, the sample-wise loss function $F(\boldsymbol{\theta}; \boldsymbol{\xi})$ is L-smooth, i.e., $\|\nabla F(\boldsymbol{\theta}; \boldsymbol{\xi}) - \nabla F(\boldsymbol{\delta}; \boldsymbol{\xi})\| \leq L\|\boldsymbol{\theta} - \boldsymbol{\delta}\|$ for all $\boldsymbol{\theta}, \boldsymbol{\delta} \in \mathbb{R}^d$.*

The Sample-Wise Smoothness Assumption 1 implies the following standard smoothness condition.

Assumption 2 (Standard Smoothness)**.** *There exists $L > 0$, such that the loss function f_i is L-smooth, i.e., $\|\nabla f_i(\boldsymbol{\theta}) - \nabla f_i(\boldsymbol{\delta})\| \leq L\|\boldsymbol{\theta} - \boldsymbol{\delta}\|$ for all $\boldsymbol{\theta}, \boldsymbol{\delta} \in \mathbb{R}^d$ and $i \in \{1, \ldots, N\}$.*

We emphasize that our original PAdaMFed algorithm is based on the Standard Smoothness Assumption 2. The slightly more stringent Assumption 1 is required when using variance reduction to further facilitate convergence.

Assumption 3 (Stochastic Gradient)**.** *There exists $\sigma \geq 0$ such that for all $\boldsymbol{\theta} \in \mathbb{R}^d$ and $i \in \{1, \ldots, N\}$, $\mathbb{E}_{\boldsymbol{\xi}_i}[\nabla F(\boldsymbol{\theta}; \boldsymbol{\xi}_i)] = \nabla f_i(\boldsymbol{\theta})$ and $\mathbb{E}_{\boldsymbol{\xi}_i} \|\nabla F(\boldsymbol{\theta}; \boldsymbol{\xi}_i) - \nabla f_i(\boldsymbol{\theta})\|^2 \leq \sigma^2$, where $\boldsymbol{\xi}_i \sim \mathcal{D}_i$.*

Assumption 3 ensures that the stochastic gradient $\nabla F(\boldsymbol{\theta}; \boldsymbol{\xi}_i)$ is unbiased and has bounded within-client variance, which is standard in stochastic optimization.

We consider nonconvex FL problems with heterogeneous data among clients that the local data distributions $\mathcal{D}_i \neq \mathcal{D}_j$ for any $i \neq j$. When addressing data heterogeneity, most existing approaches, such as SCAFFOLD (Karimireddy et al., 2020b), FedProx (Li et al., 2020), FedAMS (Chen et al., 2020), and MIME (Karimireddy et al., 2020a), require an upper bound on gradient dissimilarity, i.e., there exist constants $B, \sigma_h^2 > 0$ such that

$$\frac{1}{N} \sum_{i=1}^{N} \|\nabla f_i(\boldsymbol{\theta})\|^2 \leq B \|\nabla f(\boldsymbol{\theta})\|^2 + \sigma_h^2 \text{ for all } \boldsymbol{\theta} \in \mathbb{R}^d. \tag{1}$$

This assumption simplifies the mathematical analysis of those FL approaches and ensures their algorithmic performance. However, it may not hold in scenarios where data across clients exhibit significant and unpredictable variations, thus compromising the robustness of FL.

Existing FL algorithms typically rely on problem-specific parameters to determine their stepsizes, including the smoothness parameter L, gradient variance σ^2, and heterogeneity bounds B and σ_h^2. The smoothness parameter, which characterizes the Lipschitz continuity of gradients, is generally a global property requiring knowledge of the entire dataset. Similarly, quantifying data heterogeneity across clients necessitates a comprehensive understanding of the differences between local data distributions. However, in FL settings where raw data sharing is prohibited and only model updates are exchanged, obtaining precise measurements of these parameters is computationally prohibitive and may compromise FL's privacy guarantees.

In the subsequent section, we present an algorithm that is independent of problem-specific parameters and capable of handling arbitrarily heterogeneous data, thereby eliminating the requirement of the heterogeneity bound (1).

3 Algorithm Development

Algorithm 1 PAdaMFed: A Problem-Parameter-Agnostic Algorithm for Nonconvex FL

Require: Initial model $\boldsymbol{\theta}^0$, control variates $\boldsymbol{c}_i^{-1} = \frac{1}{K}\sum_{k=0}^{K-1} \nabla F\left(\boldsymbol{\theta}^0; \boldsymbol{\xi}_i^{-1,k}\right)$ for any i, $\boldsymbol{c}^{-1} = \frac{1}{N}\sum_i \boldsymbol{c}_i^{-1}$, momentum $\boldsymbol{g}^{-1} = \boldsymbol{c}^{-1}$, global learning rate γ, local learning rate η, and momentum parameter β
for $t = 0, \cdots, T-1$ **do**
  Central Server: Uniformly sample clients $\mathcal{S}_t \subseteq \{1, \cdots, N\}$ with $|\mathcal{S}_t| = S$
  for each client $i \in \mathcal{S}_t$ in parallel **do**
    Initialize local model $\boldsymbol{\theta}_i^{t,0} = \boldsymbol{\theta}^t$ and control variate $\boldsymbol{c}_i^t = \mathbf{0}$ (for $i \notin \mathcal{S}_t$, $\boldsymbol{c}_i^t = \boldsymbol{c}_i^{t-1}$)
    for $k = 0, \cdots, K-1$ **do**
      Compute $\boldsymbol{g}_i^{t,k} = \beta\left(\nabla F\left(\boldsymbol{\theta}_i^{t,k}; \boldsymbol{\xi}_i^{t,k}\right) - \boldsymbol{c}_i^{t-1} + \boldsymbol{c}^{t-1}\right) + (1-\beta)\boldsymbol{g}^{t-1}$
      Update local model $\boldsymbol{\theta}_i^{t,k+1} = \boldsymbol{\theta}_i^{t,k} - \eta \frac{\boldsymbol{g}_i^{t,k}}{\|\boldsymbol{g}_i^{t,k}\|}$
    end for
    Update control variate $\boldsymbol{c}_i^t = \frac{1}{K}\sum_{k=1}^{K} \nabla F\left(\boldsymbol{\theta}_i^{t,k}; \boldsymbol{\xi}_i^{t,k}\right)$
    Upload $\boldsymbol{\theta}_i^{t,K}$ and $\boldsymbol{c}_i^t$ to central server
  end for
  Central server:
  Aggregate local updates $\overline{\boldsymbol{g}}^t = \frac{1}{\eta SK}\sum_{i\in\mathcal{S}_t}\left(\boldsymbol{\theta}^t - \boldsymbol{\theta}_i^{t,K}\right)$
  Update global model $\boldsymbol{\theta}^{t+1} = \boldsymbol{\theta}^t - \gamma\overline{\boldsymbol{g}}^t$
  Aggregate control variate $\boldsymbol{c}^t = \boldsymbol{c}^{t-1} + \frac{1}{N}\sum_{i\in\mathcal{S}_t}\left(\boldsymbol{c}_i^t - \boldsymbol{c}_i^{t-1}\right)$
  Aggregate momentum $\boldsymbol{g}^t = \beta\left(\frac{1}{S}\sum_{i\in\mathcal{S}_t}\left(\boldsymbol{c}_i^t - \boldsymbol{c}_i^{t-1}\right) + \boldsymbol{c}^{t-1}\right) + (1-\beta)\boldsymbol{g}^{t-1}$
  Download $\boldsymbol{\theta}^{t+1}$ and $\beta\boldsymbol{c}^t + (1-\beta)\boldsymbol{g}^t$ to all clients
end for

In this section, we propose PAdaMFed, a problem parameter-agnostic algorithm for nonconvex FL based on adaptive stepsizes and client-side momentum. PAdaMFed is designed to operate independently of any problem-specific parameters, handle arbitrarily heterogeneous data, and accommodate partial client participation.

3.1 Algorithm Development of PAdaMFed

PAdaMFed builds upon the well-established SCAFFOLD algorithm (Karimireddy et al., 2020b), which was designed to address "client drift" in FL, where local models significantly deviate from the global model due to partial participation and data heterogeneity. The core concept of SCAFFOLD is the utilization of control variates to correct the drift between client updates and the global model. Specifically, the server maintains a global control variate, denoted by $\boldsymbol{c}^t$, to represent the average

model update direction, while each client maintains a local control variate, denoted by $\boldsymbol{c}_i^t$ for all $i \in \{1, \ldots, N\}$, to track individual update directions. Client updates are subsequently adjusted using the difference between local and global control variates. SCAFFOLD demonstrates faster and more stable convergence compared to the seminal FedAvg algorithm (McMahan et al., 2017).

In this paper, we extend the original SCAFFOLD framework by incorporating client-side momentum and local adaptive stepsizes, as outlined in Algorithm 1. Specifically, in Step 7 of Algorithm 1, the local descent direction of client i at global round t and local step k is computed as:

$$\boldsymbol{g}_i^{t,k} = \beta \left(\nabla F \left(\boldsymbol{\theta}_i^{t,k}; \boldsymbol{\xi}_i^{t,k} \right) - \boldsymbol{c}_i^{t-1} + \boldsymbol{c}^{t-1} \right) + (1-\beta) \boldsymbol{g}^{t-1}.$$

In this expression, the term $\nabla F \left(\boldsymbol{\theta}_i^{t,k}; \boldsymbol{\xi}_i^{t,k} \right)$ represents the stochastic gradient at the current local model $\boldsymbol{\theta}_i^{t,k}$ with the sample $\boldsymbol{\xi}_i^{t,k}$. The term $\boldsymbol{c}^{t-1} - \boldsymbol{c}_i^{t-1}$ adjusts the difference between the global and local control variates, helping to mitigate client drift. The term $\boldsymbol{g}^{t-1}$ denotes the current global momentum, essential for stabilizing and accelerating the convergence across clients.

In Step 8 of Algorithm 1, the local model for each client i is updated by:

$$\boldsymbol{\theta}_i^{t,k+1} = \boldsymbol{\theta}_i^{t,k} - \eta \frac{\boldsymbol{g}_i^{t,k}}{\|\boldsymbol{g}_i^{t,k}\|}.$$

Here, an adaptive stepsize $\eta / \|\boldsymbol{g}_i^{t,k}\|$ is utilized by normalizing the descent direction vector $\boldsymbol{g}_i^{t,k}$. This normalization guarantees that the updates from each client have a uniform magnitude, preventing the disproportionate impact of any individual client on the global model update. It also provides us the convenience on quantifying the distance between consecutive models in our theoretical analysis, maintaining that $\left\| \boldsymbol{\theta}_i^{t,k+1} - \boldsymbol{\theta}_i^{t,k} \right\| = \eta \left\| \boldsymbol{g}_i^{t,k} / \|\boldsymbol{g}_i^{t,k}\| \right\| = \eta$ for all i, k, t.

Additionally, since $\boldsymbol{c}_i^t = \frac{1}{K} \sum_{k=0}^{K-1} \nabla F \left(\boldsymbol{\theta}_i^{t,k}; \boldsymbol{\xi}_i^{t,k} \right)$ for all i, the momentum update in Step 16 of Algorithm 1 can be expressed as:

$$\boldsymbol{g}^t = \beta \left(\frac{1}{S} \sum_{i \in \mathcal{S}_t} \left(\frac{1}{K} \sum_{k=0}^{K-1} \nabla F \left(\boldsymbol{\theta}_i^{t,k}; \boldsymbol{\xi}_i^{t,k} \right) - \boldsymbol{c}_i^{t-1} \right) + \boldsymbol{c}^{t-1} \right) + (1-\beta) \boldsymbol{g}^{t-1}. \tag{2}$$

This equation accumulates the descent directions across clients and iterations. With $\boldsymbol{g}^t$, the optimization trajectories at each client are smoothed by the descent directions of other clients, enhancing the robustness of the optimization process against variability in local updates caused by data heterogeneity. Notably, our PAdaMFed algorithm maintains the communication workload of the SCAFFOLD for both uplink and downlink.

3.2 Accelerating PAdaMFed with Variance Reduction

Variance reduction is an effective technique to accelerate convergence and enhance the stability of FL, particularly when dealing with heterogeneous data and limited client participation. In this subsection, we enhance PAdaMFed by integrating a variance reduction component into each client's descent direction, resulting in our PAdaMFed-VR algorithm. A detailed description of this algorithm is provided in Appendix C.

PAdaMFed-VR differs from PAdaMFed primarily in its computation of the local gradient. Specifically, Step 7 of Algorithm 1 is replaced with:

$$\boldsymbol{g}_i^{t,k} = \nabla F \left(\boldsymbol{\theta}_i^{t,k}; \boldsymbol{\xi}_i^{t,k} \right) + \beta \left(\boldsymbol{c}^{t-1} - \boldsymbol{c}_i^{t-1} \right) + (1-\beta) \left(\boldsymbol{g}^{t-1} - \nabla F \left(\boldsymbol{\theta}^{t-1}; \boldsymbol{\xi}_i^{t,k} \right) \right),$$

where $\nabla F \left(\boldsymbol{\theta}^{t-1}; \boldsymbol{\xi}_i^{t,k} \right)$ represents the variance reduction component. Our variance reduction design follows the principle of STORM (Cutkosky & Orabona, 2019) to make more efficient sample utilization. For each local update, the sample $\boldsymbol{\xi}_i^{t,k}$ is used twice: 1) to compute the gradient based on the current local model $\boldsymbol{\theta}_i^{t,k}$; and 2) to evaluate the gradient at the previous global model $\boldsymbol{\theta}^{t-1}$. This dual usage of each sample mitigates the influence of within-client gradient noise, enabling more accurate estimation of gradient directions.

4 THEORETICAL RESULTS AND COMPARISONS WITH PRIOR WORK

In this section, we present theoretical analyses on the convergence properties of both PAdaMFed and PAdaMFed-VR. Based on these findings, we will compare the performance of these two algorithms with state-of-the-art FL methods.

4.1 THEORETICAL RESULTS

Theorem 1. *Suppose that Assumptions 2 and 3 hold. Let the local and global learning rates of PAdaMFed be* $\eta = \frac{1}{K\sqrt{T}}$ *and* $\gamma = \frac{(SK)^{\frac{1}{4}}}{T^{\frac{3}{4}}}$*, respectively, the momentum parameter be* $\beta = \sqrt{\frac{SK}{T}}$*, and* $\{\boldsymbol{\theta}^t\}_{t\geq 0}$ *be the iterates generated by Algorithm 1. Then, it holds for all* $T \geq 1$ *that*

$$\frac{1}{T}\sum_{t=0}^{T-1}\mathbb{E}\left\|\nabla f\left(\boldsymbol{\theta}^t\right)\right\| \leq \mathcal{O}\left(\frac{\Delta + L + \sigma + \sqrt{L\sigma}}{(SKT)^{\frac{1}{4}}} + \frac{\sqrt{SK}\sigma + L}{\sqrt{T}}\right),$$

where $\Delta := f\left(\boldsymbol{\theta}^0\right) - \min_{\boldsymbol{\theta}} f(\boldsymbol{\theta})$.

Theorem 2. *Suppose that Assumptions 1 and 3 hold. Let the local and global learning rates of PAdaMFed-VR be* $\eta = \frac{1}{KT}$ *and* $\gamma = \frac{(SK)^{\frac{1}{3}}}{T^{\frac{2}{3}}}$*, respectively, the momentum parameter be* $\beta = \frac{(SK)^{\frac{1}{3}}}{T^{\frac{2}{3}}}$*, and* $\{\boldsymbol{\theta}^t\}_{t\geq 0}$ *be the iterates generated by Algorithm 2. Then, it holds for all* $T \geq 1$ *that*

$$\frac{1}{T}\sum_{t=0}^{T-1}\mathbb{E}\left\|\nabla f\left(\boldsymbol{\theta}^t\right)\right\| \leq \mathcal{O}\left(\frac{\Delta + L + \sigma}{(SKT)^{\frac{1}{3}}} + \frac{(L+\sigma)(SK)^{\frac{1}{3}}}{T^{\frac{2}{3}}}\right).$$

Remark 1. *According to Theorem 1, PAdaMFed converges to an* ϵ*-stationary point* [1] *in expectation within* $\mathcal{O}\left(\frac{1}{SK\epsilon^4}\right)$ *communication rounds. This is improved to* $\mathcal{O}\left(\frac{1}{SK\epsilon^3}\right)$ *when incorporating variance reduction, as shown in Theorem 2. Furthermore, both algorithms demonstrate linear speedup with respect to the number of participating clients* S *and local update steps* K.

Remark 2. *In PAdaMFed, setting* $SK = \mathcal{O}(T^{\frac{1}{3}})$ *yields a sample complexity* [2] *of* $\mathcal{O}(\epsilon^{-4})$ *with a communication complexity of* $\mathcal{O}(\epsilon^{-3})$*. Similarly, by setting* $SK = \mathcal{O}(\sqrt{T})$*, PAdaMFed-VR achieves the best-known sample complexity of* $\mathcal{O}(\epsilon^{-3})$ *with a communication complexity of* $\mathcal{O}(\epsilon^{-2})$ *to find an* ϵ*-stationary point (Wu et al., 2023).*

Remark 3. *In traditional FL, selecting optimal stepsizes theoretically requires the knowledge of problem-specific parameters, which are often unavailable. Consequently, in real-world FL scenarios, stepsizes must be tuned empirically—a process that is labor-intensive, time-consuming, and sometimes even impractical. In contrast, in our PAdaMFed and PAdaMFed-VR, the stepsizes are determined by the numbers of participating clients* S*, local update steps* K*, and communication rounds* T*, eliminating the need for any problem-specific parameters. This problem-parameter-independent feature simplifies implementation, enhances robustness, and facilitates the deployment of our algorithm across diverse FL applications.*

4.2 PROOF SKETCH

Our theoretical proof starts from the L-smoothness property of the loss function $f(\boldsymbol{\theta})$, which yields the following inequality:

$$f\left(\boldsymbol{\theta}^{t+1}\right) - f\left(\boldsymbol{\theta}^t\right) \leq 2\gamma\left\|\nabla f\left(\boldsymbol{\theta}^t\right) - \boldsymbol{g}^t\right\| - \gamma\left\|\nabla f\left(\boldsymbol{\theta}^t\right)\right\| + \frac{\gamma}{SK}\sum_{i\in\mathcal{S}_t,k}\left\|\boldsymbol{g}_i^{t,k} - \boldsymbol{g}^t\right\| + \frac{\gamma^2 L}{2}.$$

[1] A point $\boldsymbol{\theta}$ is said to be ϵ-stationary if $\|\nabla f(\boldsymbol{\theta})\| \leq \epsilon$. Note that for any ϵ-stationary point defined using $\|\nabla f(\theta)\|^2$, one can derive the corresponding guarantee for $\|\nabla f(\theta)\|$ based on the following relationship:

$$\frac{1}{T}\sum_{t=1}^{T-1}\mathbb{E}\|\nabla f(\theta^t)\| = \frac{1}{T}\sum_{t=0}^{T-1}\mathbb{E}\sqrt{\|\nabla f(\theta^t)\|^2} \leq \frac{1}{T}\sum_{t=0}^{T-1}\sqrt{\mathbb{E}\|\nabla f(\theta^t)\|^2} \leq \sqrt{\frac{1}{T}\sum_{t=0}^{T-1}\mathbb{E}\|\nabla f(\theta^t)\|^2}$$

where the first and second inequalities utilizes Jensen's inequality as the square root function is concave. Therefore, we can align our results with the conventional $\frac{1}{T}\sum_{t=1}^{T}\|\nabla f(\theta^t)\|^2$ metric by taking square root on both sides of their convergence bounds.

[2] Total number of samples across clients, local updates, and communication rounds.

To establish an upper bound for $\frac{1}{T}\sum_{t=0}^{T-1}\mathbb{E}\left\|\nabla f\left(\boldsymbol{\theta}^t\right)\right\|$, we must quantify two key terms: $\frac{1}{T}\sum_{t=0}^{T-1}\mathbb{E}\left\|\nabla f\left(\boldsymbol{\theta}^t\right)-\boldsymbol{g}^t\right\|$ and $\frac{1}{T}\sum_{t=0}^{T-1}\frac{1}{SK}\mathbb{E}\left[\sum_{i\in\mathcal{S}_t,k}\left\|\boldsymbol{g}_i^{t,k}-\boldsymbol{g}^t\right\|\right]$.

The momentum $\boldsymbol{g}^t$ is a recursive variable that accumulates values from previous rounds. By plugging into the expression of $\boldsymbol{g}^t$ (provided in (2)) into $\left|\nabla f\left(\boldsymbol{\theta}^t\right)-\boldsymbol{g}^t\right|$ and introducing the auxiliary term $f\left(\boldsymbol{\theta}^{t-1}\right)$, we can recursively express $\left\|\nabla f\left(\boldsymbol{\theta}^t\right)-\boldsymbol{g}^t\right\|$ by its predecessor $\left\|\nabla f\left(\boldsymbol{\theta}^{t-1}\right)-\boldsymbol{g}^{t-1}\right\|$, scaled by a contraction coefficient $(1-\beta)$. This substitution also introduces additional terms associated with stochastic gradients and control variates. Through meticulous control of all intermediate terms, we prove that $\frac{1}{T}\sum_{t=0}^{T-1}\mathbb{E}\left\|\nabla f\left(\boldsymbol{\theta}^t\right)-\boldsymbol{g}^t\right\|$ is upper bounded by $\mathcal{O}((SKT)^{-\frac{1}{4}})$ for PAdaMFed and by $\mathcal{O}((SKT)^{-\frac{1}{3}})$ for PAdaMFed-VR.

The term $\mathbb{E}\left[\sum_{i\in\mathcal{S}t,k}\left\|\boldsymbol{g}_i^{t,k}-\boldsymbol{g}^t\right\|\right]$ represents gradient dissimilarity across clients. While the heterogeneity bound (1) could readily control this term, our objective is to eliminate dependence on such bounds. Instead, we relax this term to $\mathbb{E}\left\|\nabla f_i\left(\boldsymbol{\theta}^{t-1}\right)-\boldsymbol{c}_i^{t-1}\right\|$, along with other controllable terms, by substituting the expressions for $\boldsymbol{g}_i^{t,k}$ and $\boldsymbol{g}^t$. Analogous to our treatment of $\mathbb{E}\left|\nabla f\left(\boldsymbol{\theta}^t\right)-\boldsymbol{g}^t\right|$, we exploit the recursive property of the control variate $\boldsymbol{c}_i^{t-1}$ to bound $\mathbb{E}\left\|\nabla f_i\left(\boldsymbol{\theta}^{t-1}\right)-\boldsymbol{c}_i^{t-1}\right\|$. This, in turn, allows us to establish a bound for $\mathbb{E}\left[\sum_{i\in\mathcal{S}_t,k}\left\|\boldsymbol{g}_i^{t,k}-\boldsymbol{g}^t\right\|\right]$.

Combining the above processes leads to our analytical results. For comprehensive proofs, please refer to Appendix B for Theorem 1 and Appendix C for Theorem 2.

Intuition on the Algorithmic Features: The efficacy of PAdaMFed stems from the synergistic integration of three indispensable components: local gradient normalization, client-side momentum, and control variates. 1) Gradient normalization serves as an adaptive learning rate scheme, automatically adjusting stepsizes based on the local optimization landscape. This design automatically allows larger steps in regions with small gradients (where more aggressive exploration is beneficial) and smaller steps in steep regions (where careful progress is needed). 2) Client-side momentum helps accelerate convergence while maintaining stability. First, it helps overcome local irregularities in the loss landscape by accumulating gradients over clients and iterations; Second, it accelerates progress in directions of consistent gradient agreement. 3) Furthermore, control variates align local updates with the global objective, reducing variance in gradient estimates and ensuring more consistent updates across heterogeneous client data. Collectively, these techniques ensure that the stepsizes are independent of problem-specific parameters such as smoothness parameters and heterogeneity bounds, simplifying the tuning process and enhancing robustness across diverse FL applications. Notably, our algorithms also eliminate the need for data heterogeneity bounds, further broadening their applicability.

4.3 Comparisons with Prior Work

We compare PAdaMFed and PAdaMFed-VR with several representative algorithms for solving FL problems with heterogeneous data, as listed in Table 1.

Comparisons of PAdaMFed with Prior FL Algorithms: The SCAFFOLD (Karimireddy et al., 2020b) algorithm requires the smoothness parameter L for stepsize tuning. However, its communication complexity, given by $\mathcal{O}\left(\left(\frac{N}{S}\right)^{\frac{1}{3}}\frac{L}{K\epsilon^4}\right)$, is suboptimal. MIME (Karimireddy et al., 2020a) improves this complexity to $\mathcal{O}\left(\frac{1}{SK\epsilon^4}\right)$ by incorporating server-level momentum. Nevertheless, MIME requires large-batch local gradients per round, and its learning rates depend on multiple problem parameters, including initial optimality gap Δ and heterogeneity bound σ_h^2, which are challenging to estimate.

FedSPS (Sohom Mukherjee, 2024) incorporates stochastic Polyak step-sizes into local client updates, achieving a communication complexity of $\mathcal{O}\left(\frac{1}{NK\epsilon^4}\right)$ in full participation scenarios. However, its analysis relies on the assumption of bounded data heterogeneity. Moreover, its stepsize tuning requires knowledge of the lower bounds of all local loss functions, i.e., ℓ_i^* for all i, in addition to the smoothness parameter L, leading to significant problem-parameter dependence.

SCAFFOLD-M (Cheng et al., 2024) employs similar client-side momentum as PAdaMFed, removing the need for bounded data heterogeneity. However, SCAFFOLD-M's stepsizes depend on sev-

Table 1: Comparisons of algorithms for solving FL problems with heterogeneous data. (Shorthand notation: Add. Assump. = Additional assumptions aside from Assumptions 1–3, BDH = Bounded data heterogeneity define in (1), BG = Bounded gradient that $\|\nabla f_i(\boldsymbol{\theta})\| \leq G,\ \forall i, \boldsymbol{\theta}$, BHD = Bounded Hessian dissimilarity that $\left\|\nabla^2 f_i(\boldsymbol{\theta}) - \nabla^2 f(\boldsymbol{\theta})\right\|^2 \leq \delta,\ \forall i, \boldsymbol{\theta}$)

Algorithms	**Add. Assump.**	**Stepsize**	**Stepsize-Related Problem Parameters**	**Communication Complexity**
SCAFFOLD (Karimireddy et al., 2020b)	–	$\gamma = \sqrt{S}, \eta \leq \frac{1}{24\gamma KL}\left(\frac{S}{N}\right)^{\frac{2}{3}}$	L	$\mathcal{O}\left(\left(\frac{N}{S}\right)^{\frac{1}{3}}\frac{L}{K\epsilon^4}\right)$
MIME (Karimireddy et al., 2020a)	BDH, BHD	$\eta = \sqrt{\frac{\Delta S}{L\tilde{G}TK^2}}, \tilde{G} = \sigma_h^2 + \frac{\sigma^2}{K}$	$L, \Delta, \sigma^2, \sigma_h^2$	$\mathcal{O}\left(\frac{1}{SK\epsilon^4}\right)$
FedSPS (Sohom Mukherjee, 2024)	BDH	$\eta_i^{t,k} = \min\left\{\frac{F\left(\boldsymbol{\theta}_i^{t,k};\boldsymbol{\xi}_i^{t,k}\right)-\ell_i^*}{c\left\|\nabla F\left(\boldsymbol{\theta}_i^{t,k};\boldsymbol{\xi}_i^{t,k}\right)\right\|^2}, \eta_b\right\}$[1] $\eta_b \leq \min\left\{\frac{1}{2cL}, \frac{1}{25LK}\right\}$	$L, \ell_i^*, \forall i$	$\mathcal{O}\left(\frac{1}{NK\epsilon^4}\right)$
SCAFFOLD-M (Cheng et al., 2024)	–	$\beta = \min\left\{1, \frac{S}{N^{\frac{2}{3}}}, \sqrt{\frac{L\Delta SK}{\sigma^2 T}}, \sqrt{\frac{L\Delta S^2}{G_0 N}}\right\}$[2] $\gamma = \frac{\beta}{L}, \eta KL \lesssim \min\left\{\frac{1}{\sqrt{S}}, \frac{1}{\beta K^{\frac{1}{4}}}, \frac{\sqrt{S}}{N}\right\}$	L, Δ, σ^2, G_0	$\mathcal{O}\left(\frac{1}{SK\epsilon^4}\right)$
PAdaMFed (This paper)	–	$\beta = \sqrt{\frac{SK}{T}}, \gamma = \frac{(SK)^{\frac{1}{4}}}{T^{\frac{3}{4}}}, \eta = \frac{1}{K\sqrt{T}}$	–	$\mathcal{O}\left(\frac{1}{SK\epsilon^4}\right)$
Variance-Reduced				
FAFED (Wu et al., 2023)	BDH, BG	$\eta_t \propto \frac{N^{\frac{2}{3}}}{Lt^{\frac{1}{3}}}, \beta_t \propto \eta_t^2$	L	$\mathcal{O}\left(\frac{1}{SK\epsilon^3}\right)$
SCAFFOLD-M-VR (Cheng et al., 2024)	–	$\beta = \min\left\{\frac{S}{N}, \left(\frac{KL\Delta}{\sigma^2 T}\right)^{\frac{2}{3}}, S^{\frac{1}{3}}\right\}$ $\gamma L = \min\left\{1, \sqrt{\beta S}\right\}$ $\eta KL \lesssim \min\left\{\sqrt{\frac{\beta}{S}}, \left(\frac{\beta}{SK}\right)^{\frac{1}{4}}\right\}$	L, Δ, σ^2	$\mathcal{O}\left(\frac{1}{S\sqrt{K}\epsilon^4}\right)$
PAdaMFed-VR (This paper)	–	$\beta = \frac{(SK)^{\frac{1}{3}}}{T^{\frac{2}{3}}}, \gamma = \frac{(SK)^{\frac{1}{3}}}{T^{\frac{2}{3}}}, \eta = \frac{1}{KT}$	–	$\mathcal{O}\left(\frac{1}{SK\epsilon^3}\right)$

[1] $\ell_i^* \leq \inf_{\boldsymbol{\theta}, \boldsymbol{\xi}_i \sim \mathcal{D}_i} F(\boldsymbol{\theta}; \boldsymbol{\xi}_i)$ for any i, and c is a constant to balance adaptivity and accuracy.
[2] $G_0 := \frac{1}{N}\sum_{i=1}^N \left\|\nabla f_i(\boldsymbol{\theta}^0)\right\|^2$.

eral problem-specific parameters, including the smoothness parameter L, initial optimal gap Δ, and stochastic gradient variance σ^2, resulting in laborious stepsize tuning. In contrast, PAdaMFed is completely independent of problem-specific parameters.[3]

Comparisons of PAdaMFed-VR with Prior Variance-Reduced FL Algorithms: FAFED (Wu et al., 2023) employing a momentum-based variance reduction with an adaptive matrix, achieving the best-known $\mathcal{O}(\epsilon^{-3})$ sample complexity and $\mathcal{O}(\epsilon^{-2})$ communication complexity through the use of diminishing stepsizes. However, FAFED requires stringent assumptions of bounded gradients and bounded data heterogeneity. Moreover, its learning rates are subject to several complex constraints and rely on problem-parameter-based algorithm tuning. SCAFFOLD-M-VR (Cheng et al., 2024) is a variance-reduced SCAFFOLD-M algorithm and, similarly, requires careful step size tuning

[3] It is worth mentioning that SCAFFOLD-M achieves a convergence rate of $\frac{1}{T}\sum_{r=0}^{T-1}\mathbb{E}[\|\nabla f(\boldsymbol{\theta}^t)\|^2] \leq \mathcal{O}\left(\sqrt{\frac{L\Delta\sigma^2}{SKT}} + \frac{L\Delta}{T}\left(1 + \frac{N^{2/3}}{S}\right)\right)$. While this bound is theoretically superior to our method by a factor of $\frac{N^{2/3}}{S}$ in the second term, the overall convergence behavior is primarily governed by the first term. Therefore, our comparative analysis focuses on the dominant first term, which represents the primary bottleneck in practical convergence.

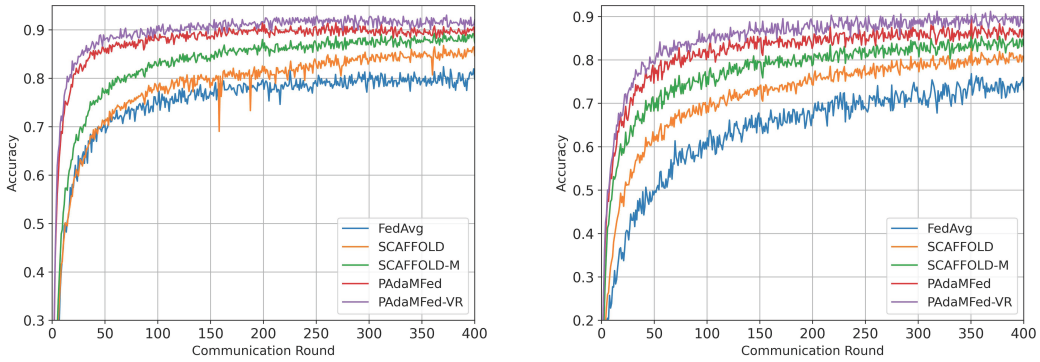

(a) i.i.d (b) non-i.i.d

Figure 1: Test accuracy versus the number of communication rounds on the EMNIST dataset.

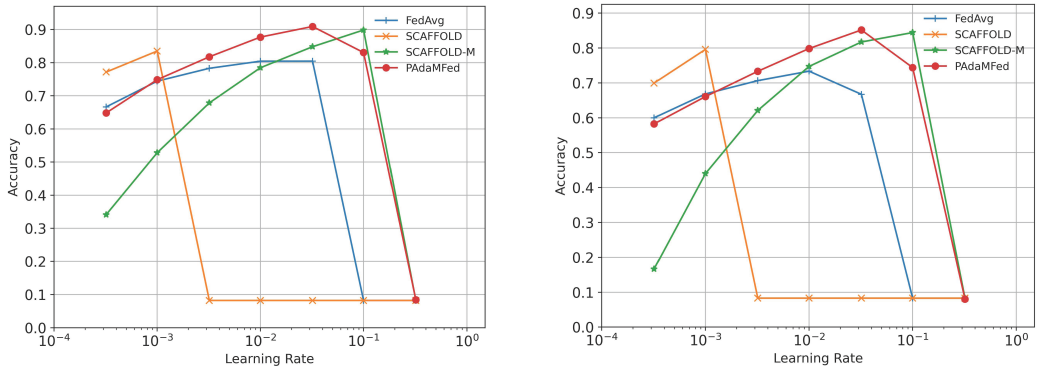

(a) i.i.d (b) non-i.i.d

Figure 2: Test accuracy versus learning rate on the EMNIST dataset.

based on multiple problem-dependent parameters. Even though, it fails to achieve the best-known complexity established in the literature.

5 Numerical Experiments

In this section, we present experiments on two distinct tasks: image classification and textual sentiment analysis. The image classification task is performed on both the EMNIST dataset (Cohen et al., 2017) and the CIFAR-10 (Li et al., 2017) dataset , while the sentiment analysis task is conducted on the IMDB dataset (Maas et al., 2011), which contains movie reviews sourced from the Internet Movie Database. We evaluate the proposed algorithms against baselines, including FedAvg (McMahan et al., 2017), SCAFFOLD (Karimireddy et al., 2020b), and SCAFFOLD-M (Cheng et al., 2024). Additionally, experiments are conducted under both i.i.d. and non-i.i.d. data settings. Due to space limitations, the detailed experimental setup and additional simulation results are provided in Appendix D.

Figure 1 illustrates the test accuracy of various algorithms versus the number of communication rounds on the EMNIST dataset, with subfigure 1a representing i.i.d. data and subfigure 1b depicting non-i.i.d. data. The stepsizes for our algorithms, PAdaMFed and PAdaMFed-VR, are determined based on the theoretical guidance provided in Theorem 1 and Theorem 2, respectively. For fair comparisons, the hyperparameters of other algorithms in Figure 1 are optimized through grid search to achieve their best performance. The results demonstrate that our proposed methods significantly outperform all baseline algorithms—FedAvg, SCAFFOLD, and SCAFFOLD-M—in both convergence speed and test accuracy. Notably, although SCAFFOLD-M employs a similar momentum technique, it converges more slowly than PAdaMFed and achieves lower accuracy, validating the efficacy of our adaptive stepsize design. Building upon these advantages, the incorporation of variance reduction further enhances our methods' superiority through more efficient sample utilization. Moreover, the

results on non-i.i.d. data in subfigure 1b demonstrate even greater performance margins than the i.i.d. case, highlighting the advantages of our algorithms.

Figure 2 compares the test accuracy of various algorithms versus the learning rate on the EMNIST dataset. All algorithms were evaluated over 400 communication rounds to ensure fair comparison. We observe that our algorithm demonstrates superior robustness to stepsize selection, maintaining stable performance across a significantly wider range of learning rates compared to baseline methods. Specifically, it achieves test accuracy exceeding 0.8 across the stepsize range $[3 \times 10^{-3}, 10^{-1}]$ for i.i.d. data distributions (subfigure 2a) and above 0.7 for the same stepsize range under non-i.i.d. conditions (subfigure 2b). In contrast, baseline algorithms exhibit substantially narrower regions of stable performance, empirically validating our method's enhanced stepsize robustness.

6 Conclusions

This paper has proposed an innovative approach to eliminating problem-specific parameter dependencies in FL, enabling parameter-agnostic generalization across diverse settings. Our algorithms have also removed the need for data heterogeneity bounds and accommodated partial client participation, further broadening its applicability to real-world scenarios. We have provided a rigorous theoretical analysis demonstrating state-of-the-art convergence rate, based on the minimal assumptions of L-smoothness of loss functions and unbiased stochastic gradients with bounded within-client variance. Additionally, we have enhanced the convergence rate of our algorithm through variance reduction, achieving the best-known $\mathcal{O}(\epsilon^{-3})$ sampling complexity and $\mathcal{O}(\epsilon^{-2})$ communication complexity. Furthermore, we have provided extensive numerical evidence on both image classification and textual sentiment analysis tasks to verify the efficacy of our approaches.

References

Durmus Alp Emre Acar, Yue Zhao, Ramon Matas Navarro, Matthew Mattina, Paul N Whatmough, and Venkatesh Saligrama. Federated learning based on dynamic regularization. *arXiv preprint arXiv:2111.04263*, 2021.

Sulaiman A Alghunaim. Local exact-diffusion for decentralized optimization and learning. *IEEE Transactions on Automatic Control*, 2024.

Mingzhe Chen, Nir Shlezinger, H Vincent Poor, Yonina C Eldar, and Shuguang Cui. Communication-efficient federated learning. *Proceedings of the National Academy of Sciences*, 118(17):e2024789118, 2021.

Xiangyi Chen, Xiaoyun Li, and Ping Li. Toward communication efficient adaptive gradient method. In *Proceedings of the 2020 ACM-IMS on Foundations of Data Science Conference*, pp. 119–128, 2020.

Ziheng Cheng, Xinmeng Huang, and Kun Yuan. Momentum benefits non-iid federated learning simply and provably. *The Twelfth International Conference on Learning Representations.*, 2024.

Gregory Cohen, Saeed Afshar, Jonathan Tapson, and Andre Van Schaik. Emnist: Extending mnist to handwritten letters. In *2017 international joint conference on neural networks (IJCNN)*, pp. 2921–2926. IEEE, 2017.

Ashok Cutkosky and Francesco Orabona. Momentum-based variance reduction in non-convex SGD. *Advances in neural information processing systems*, 32, 2019.

Yuyang Deng, Mohammad Mahdi Kamani, and Mehrdad Mahdavi. Adaptive personalized federated learning. *arXiv preprint arXiv:2003.13461*, 2020.

John Duchi, Elad Hazan, and Yoram Singer. Adaptive subgradient methods for online learning and stochastic optimization. *Journal of machine learning research*, 12(7), 2011.

Huimin Gao, Qingtao Wu, Xuhui Zhao, Junlong Zhu, and Mingchuan Zhang. Fedadt: An adaptive method based on derivative term for federated learning. *Sensors*, 23(13):6034, 2023.

Geoffrey Hinton. Neural networks for machine learning, lecture 6a, 2012. URL http://www.cs.toronto.edu/~tijmen/csc321/slides/lecture_slides_lec6.pdf. Coursera.

Tzu-Ming Harry Hsu, Hang Qi, and Matthew Brown. Measuring the effects of non-identical data distribution for federated visual classification. *arXiv preprint arXiv:1909.06335*, 2019.

Sai Praneeth Karimireddy, Martin Jaggi, Satyen Kale, Mehryar Mohri, Sashank J Reddi, Sebastian U Stich, and Ananda Theertha Suresh. Mime: Mimicking centralized stochastic algorithms in federated learning. *arXiv preprint arXiv:2008.03606*, 2020a.

Sai Praneeth Karimireddy, Satyen Kale, Mehryar Mohri, Sashank Reddi, Sebastian Stich, and Ananda Theertha Suresh. Scaffold: Stochastic controlled averaging for federated learning. In *International conference on machine learning*, pp. 5132–5143. PMLR, 2020b.

Diederik P Kingma and Jimmy Ba. Adam: A method for stochastic optimization. *arXiv preprint arXiv:1412.6980*, 2014.

Anastasia Koloskova, Nicolas Loizou, Sadra Boreiri, Martin Jaggi, and Sebastian Stich. A unified theory of decentralized SGD with changing topology and local updates. In *International Conference on Machine Learning*, pp. 5381–5393. PMLR, 2020.

Jakub Konečnỳ, H Brendan McMahan, Felix X Yu, Peter Richtárik, Ananda Theertha Suresh, and Dave Bacon. Federated learning: Strategies for improving communication efficiency. *arXiv preprint arXiv:1610.05492*, 2016.

Hongmin Li, Hanchao Liu, Xiangyang Ji, Guoqi Li, and Luping Shi. Cifar10-dvs: an event-stream dataset for object classification. *Frontiers in neuroscience*, 11:309, 2017.

Jiaxiang Li, Xuxing Chen, Shiqian Ma, and Mingyi Hong. Problem-parameter-free decentralized nonconvex stochastic optimization. *arXiv preprint arXiv:2402.08821*, 2024.

Tian Li, Anit Kumar Sahu, Manzil Zaheer, Maziar Sanjabi, Ameet Talwalkar, and Virginia Smith. Federated optimization in heterogeneous networks. *Proceedings of Machine learning and systems*, 2:429–450, 2020.

Xiaoxiao Li, Meirui Jiang, Xiaofei Zhang, Michael Kamp, and Qi Dou. Fedbn: Federated learning on non-iid features via local batch normalization. *arXiv preprint arXiv:2102.07623*, 2021.

Xianfeng Liang, Shuheng Shen, Jingchang Liu, Zhen Pan, Enhong Chen, and Yifei Cheng. Variance reduced local SGD with lower communication complexity. *arXiv preprint arXiv:1912.12844*, 2019.

Andrew Maas, Raymond E Daly, Peter T Pham, Dan Huang, Andrew Y Ng, and Christopher Potts. Learning word vectors for sentiment analysis. In *Proceedings of the 49th annual meeting of the association for computational linguistics: Human language technologies*, pp. 142–150, 2011.

Brendan McMahan, Eider Moore, Daniel Ramage, Seth Hampson, and Blaise Aguera y Arcas. Communication-efficient learning of deep networks from decentralized data. In *Artificial intelligence and statistics*, pp. 1273–1282. PMLR, 2017.

Hesham Mostafa. Robust federated learning through representation matching and adaptive hyperparameters. *arXiv preprint arXiv:1912.13075*, 2019.

Viraaji Mothukuri, Reza M Parizi, Seyedamin Pouriyeh, Yan Huang, Ali Dehghantanha, and Gautam Srivastava. A survey on security and privacy of federated learning. *Future Generation Computer Systems*, 115:619–640, 2021.

Sashank Reddi, Zachary Charles, Manzil Zaheer, Zachary Garrett, Keith Rush, Jakub Konečnỳ, Sanjiv Kumar, and H Brendan McMahan. Adaptive federated optimization. *arXiv preprint arXiv:2003.00295*, 2020.

Felix Sattler, Simon Wiedemann, Klaus-Robert Müller, and Wojciech Samek. Robust and communication-efficient federated learning from non-iid data. *IEEE transactions on neural networks and learning systems*, 31(9):3400–3413, 2019.

Sebastian U. Stich Sohom Mukherjee, Nicolas Loizou. Locally adaptive federated learning. *arXiv preprint arXiv:2307.06306*, 2024.

Jianyu Wang, Vinayak Tantia, Nicolas Ballas, and Michael Rabbat. Slowmo: Improving communication-efficient distributed SGD with slow momentum. *arXiv preprint arXiv:1910.00643*, 2019.

Jianyu Wang, Qinghua Liu, Hao Liang, Gauri Joshi, and H Vincent Poor. Tackling the objective inconsistency problem in heterogeneous federated optimization. *Advances in neural information processing systems*, 33:7611–7623, 2020.

Xiaolu Wang, Yuchang Sun, Hoi-To Wai, and Jun Zhang. Dual-delayed asynchronous sgd for arbitrarily heterogeneous data. *arXiv preprint arXiv:2405.16966*, 2024.

Kang Wei, Jun Li, Ming Ding, Chuan Ma, Howard H Yang, Farhad Farokhi, Shi Jin, Tony QS Quek, and H Vincent Poor. Federated learning with differential privacy: Algorithms and performance analysis. *IEEE transactions on information forensics and security*, 15:3454–3469, 2020.

Xidong Wu, Feihu Huang, Zhengmian Hu, and Heng Huang. Faster adaptive federated learning. In *Proceedings of the AAAI conference on artificial intelligence*, volume 37, pp. 10379–10387, 2023.

Chenhao Xu, Youyang Qu, Yong Xiang, and Longxiang Gao. Asynchronous federated learning on heterogeneous devices: A survey. *Computer Science Review*, 50:100595, 2023.

Jing Xu, Sen Wang, Liwei Wang, and Andrew Chi-Chih Yao. Fedcm: Federated learning with client-level momentum. *arXiv preprint arXiv:2106.10874*, 2021.

A Related Works

Adaptive Stepsize Methods: Adaptive stepsize methods have gained significant attention in optimization literature due to their ability to automatically adjust learning rates based on the geometry of the objective function. These methods, such as Adam (Kingma & Ba, 2014), AdaGrad (Duchi et al., 2011), and RMSProp (Hinton, 2012), have demonstrated remarkable success in various machine learning tasks, particularly in handling sparse gradients and non-stationary objectives. In the context of FL, adaptive stepsizes offer several advantages. First, they eliminate the need for manual tuning of learning rates, which is especially beneficial in federated settings where global knowledge of the objective function's properties is limited. Second, adaptive methods can potentially mitigate the impact of data heterogeneity by allowing different update rates for different model parameters, effectively accounting for varying gradient statistics across clients.

FedOpt (Reddi et al., 2020) introduced adaptive optimization techniques like AdaGrad, Adam, and Yogi into FL, demonstrating improved convergence properties compared to the traditional FedAvg algorithm. Wang et al. (2020) proposed FedNova, which normalizes and scales local updates to mitigate objective inconsistency caused by partial client participation and data heterogeneity. FedBN (Li et al., 2021) employed local batch normalization to alleviate feature shift before averaging models, outperforming both classical FedAvg (McMahan et al., 2017) and FedProx (Li et al., 2020) for non-IID data. While these approaches demonstrated the advantages of adaptive methods for easing parameter tuning, none provides theoretical guarantees, and careful tuning of global learning rates remains essential.

Momentum: Momentum, on the other hand, is a technique that accelerates gradient descent by maintaining a velocity vector that captures the history of gradients. In nonconvex optimization, momentum has been shown to help escape saddle points more efficiently and potentially reach better local optima (Cutkosky & Orabona, 2019). The incorporation of momentum in FL algorithms can provide several benefits. It can help smooth out the impact of heterogeneous updates from different clients, potentially leading to more stable and faster convergence. Moreover, momentum can aid in overcoming the challenges posed by partial client participation by maintaining a consistent optimization trajectory even when client participation varies across rounds.

Hsu et al. (2019) proposed FedAvgM, which adds a server-side momentum term to the FedAvg algorithm, demonstrating improved convergence rates and robustness to data heterogeneity. Wang et al. (2019) developed SlowMo, a momentum-based method using two nested loops to achieve faster convergence in distributed optimization. Both FedCM (Xu et al., 2021) and (Cheng et al., 2024) investigated the integration of client-side momentum in FedAvg to effectively tackle client heterogeneity and partial participation in FL.

Combination of Adaptive Stepsizes and Momentum: Recent works have explored combining adaptive methods and momentum in FL. FedAMS (Chen et al., 2020) implements a local AMSGrad scheme for FL, demonstrating fast convergence with low communication cost. MIme (Karimireddy et al., 2020a) combines control-variates with server-level momentum at every local update to mimic centralized methods running on IID data, outperforming centralized methods but requiring a large-batch local gradient per round for each client. Wu et al. (2023) introduced FAFED, a momentum-based variance reduction scheme integrated with an adaptive matrix, attaining the best-known sample and communication complexity when using diminishing stepsizes. While these methods demonstrate improved performance, they still require careful tuning of global learning rates.

A recent contribution, FedSPS (Sohom Mukherjee, 2024), claims to be the first fully locally adaptive method for FL with minimal hyperparameter tuning. While promising, this approach relies on stringent assumptions of bounded data heterogeneity and gradients. Moreover, it fails to converge to optima with constant stepsizes and requires adjustment of a maximum stepsize threshold based on the smoothness parameter, thus retaining some hyperparameter dependence. The limitations of existing approaches underscore the critical need for more robust, adaptive FL algorithms capable of operating effectively across diverse scenarios without extensive parameter tuning.

This paper makes a significant advancement by proposing a novel algorithm, PAdaMFed, that completely eliminates dependency on problem-specific parameters. All stepsizes in our approach are explicitly determined by the number of participating clients, local updates, and communication rounds.

To the best of our knowledge, this is the first algorithm that achieves such problem-parameter independence in FL. Moreover, our algorithm inherently manages data heterogeneity and partial client participation without requiring any heterogeneity bound among clients, which is also nontrivial.

Data heterogeneity has been extensively studied in FL. However, existing algorithms either depend on bounded data heterogeneity (e.g., FedAvg (McMahan et al., 2017), SCAFFOLD (Karimireddy et al., 2020b), FedProx (Li et al., 2020), and MIme (Karimireddy et al., 2020a)) or fall short of achieving state-of-the-art convergence rates (e.g., VRL-SGD (Liang et al., 2019) and LED (Alghunaim, 2024)). Recently, Cheng et al. (2024) demonstrated that momentum can eliminate the data heterogeneity constraint in the FedAvg and SCAFFOLD algorithms while achieving state-of-the-art convergence results. Wang et al. (2024) introduced DuDe-ASGD for asynchronous FL, which can effectively handle arbitrarily heterogeneous data by leveraging stale stochastic gradients. However, their algorithms require carefully designed stepsizes based on hyperparameters. In contrast, our algorithm accommodates arbitrary data heterogeneity while achieving complete problem-parameter independence.

A notable concurrent work by (Li et al., 2024) also explores problem-parameter free algorithms in the context of decentralized non-convex optimization. While both studies target problem-parameter free optimization, our work addresses the unique challenges inherent to federated learning settings. The fundamental distinction lies in our treatment of client drift—a critical phenomenon arising from multiple local updates and data heterogeneity in federated environments. Our key technical contributions beyond (Li et al., 2024) are twofold: 1) The development of a novel framework integrating control variates with momentum to mitigate client drift, requiring sophisticated theoretical analysis due to their complex interactions; 2) The successful elimination of explicit heterogeneity bounds, which were previously considered essential in federated learning literature.

B Theoretical Analysis of PAdaMFed

Our analysis is based on the following useful lemmas.

Lemma 1. *For any t, we have*

$$\frac{1}{NK}\sum_{i,k}\left\|\boldsymbol{\theta}_i^{t,k}-\boldsymbol{\theta}^t\right\|^2 \le \frac{1}{3}\eta^2K^2 \quad \textit{and} \quad \frac{1}{NK}\sum_{i,k}\left\|\boldsymbol{\theta}_i^{t,k}-\boldsymbol{\theta}^t\right\| \le \frac{1}{2}\eta K.$$

Proof. From the update rule of local model, for any i, k and t, we have

$$\left\|\boldsymbol{\theta}_i^{t,k+1}-\boldsymbol{\theta}_i^{t,k}\right\| = \eta\left\|\frac{\boldsymbol{g}_i^{t,k}}{\left\|\boldsymbol{g}_i^{t,k}\right\|}\right\| \le \eta.$$

Then,

$$\left\|\boldsymbol{\theta}_i^{t,k}-\boldsymbol{\theta}^t\right\|^2 = \left\|\sum_{j=0}^{k-1}\left(\boldsymbol{\theta}_i^{t,j+1}-\boldsymbol{\theta}_i^{t,j}\right)\right\|^2 \le k\sum_{j=0}^{k-1}\left\|\boldsymbol{\theta}_i^{t,j+1}-\boldsymbol{\theta}_i^{t,j}\right\|^2 \le \eta^2k^2.$$

Summing the above inequality over i and k yields

$$\frac{1}{NK}\sum_{i,k}\left\|\boldsymbol{\theta}_i^{t,k}-\boldsymbol{\theta}^t\right\|^2 \le \frac{\eta^2}{K}\sum_{k=0}^{K-1}k^2 \le \frac{\eta^2}{6K}(K-1)K(2K-1) \le \frac{1}{3}\eta^2K^2.$$

Similarly, we have

$$\frac{1}{NK}\sum_{i,k}\left\|\boldsymbol{\theta}_i^{t,k}-\boldsymbol{\theta}^t\right\| \le \frac{1}{NK}\sum_{i,k}\left(\mathbb{E}\left\|\boldsymbol{\theta}_i^{t,k}-\boldsymbol{\theta}^t\right\|^2\right)^{\frac{1}{2}} \le \frac{\eta}{K}\sum_{k=0}^{K-1}k \le \frac{1}{2}\eta K.$$

□

These inequalities in Lemma 1 are frequently used in our analysis.

Lemma 2. *Given vectors $\boldsymbol{\omega}_1, \cdots, \boldsymbol{\omega}_N \in \mathbb{R}^d$ and $\overline{\boldsymbol{\omega}} = \frac{1}{N}\sum_{i=1}^N \boldsymbol{\omega}_i$, if we sample $\mathcal{S} \subset \{1, \cdots, N\}$ uniformly randomly such that $|\mathcal{S}| = S$, then it holds that*

$$\mathbb{E}\left[\left\|\frac{1}{S}\sum_{i\in\mathcal{S}}\boldsymbol{\omega}_i\right\|^2\right] \leq \|\overline{\boldsymbol{\omega}}\|^2 + \frac{1}{SN}\sum_{i=1}^N \|\boldsymbol{\omega}_i - \overline{\boldsymbol{\omega}}\|^2.$$

Proof. Letting $\mathbb{1}\{i \in \mathcal{S}\}$ be the indicator for the event $i \in \mathcal{S}$, we prove this lemma by direct calculation as follows:

$$\begin{aligned}
\mathbb{E}\left[\left\|\frac{1}{S}\sum_{i\in\mathcal{S}}\boldsymbol{\omega}_i\right\|^2\right] &= \mathbb{E}\left[\left\|\frac{1}{S}\sum_{i=1}^N\boldsymbol{\omega}_i\mathbb{1}\{i\in\mathcal{S}\}\right\|^2\right] \\
&= \frac{1}{S^2}\mathbb{E}\left[\left(\sum_i \|\boldsymbol{\omega}_i\|^2 \mathbb{1}\{i\in\mathcal{S}\} + 2\sum_{i<j}\boldsymbol{\omega}_i^\top\boldsymbol{\omega}_j\mathbb{1}\{i,j\in\mathcal{S}\}\right)\right] \\
&= \frac{1}{SN}\sum_{i=1}^N\|\boldsymbol{\omega}_i\|^2 + \frac{1}{S^2}\frac{S(S-1)}{N(N-1)}2\sum_{i<j}\boldsymbol{\omega}_i^\top\boldsymbol{\omega}_j \\
&= \frac{1}{SN}\sum_{i=1}^N\|\boldsymbol{\omega}_i\|^2 + \frac{1}{S^2}\frac{S(S-1)}{N(N-1)}\left(\left\|\sum_{i=1}^N\boldsymbol{\omega}_i\right\|^2 - \sum_{i=1}^N\|\boldsymbol{\omega}_i\|^2\right) \\
&= \frac{N-S}{S(N-1)}\frac{1}{N}\sum_{i=1}^N\|\boldsymbol{\omega}_i\|^2 + \frac{N(S-1)}{S(N-1)}\|\overline{\boldsymbol{\omega}}\|^2 \\
&= \frac{N-S}{S(N-1)}\frac{1}{N}\sum_{i=1}^N\|\boldsymbol{\omega}_i - \overline{\boldsymbol{\omega}}\|^2 + \|\overline{\boldsymbol{\omega}}\|^2 \\
&\leq \frac{1}{SN}\sum_{i=1}^N\|\boldsymbol{\omega}_i - \overline{\boldsymbol{\omega}}\|^2 + \|\overline{\boldsymbol{\omega}}\|^2,
\end{aligned}$$

where the last inequality uses the fact that $\frac{N-S}{N-1} \leq 1$ for any nonempty set $\mathcal{S}$. □

From the L-smoothness of $f(\cdot)$ in Assumption 2, we have

$$\begin{aligned}
&f\left(\boldsymbol{\theta}^{t+1}\right) - f\left(\boldsymbol{\theta}^t\right) \\
&\leq \nabla f\left(\boldsymbol{\theta}^t\right)^\top\left(\boldsymbol{\theta}^{t+1} - \boldsymbol{\theta}^t\right) + \frac{L}{2}\left\|\boldsymbol{\theta}^{t+1} - \boldsymbol{\theta}^t\right\|^2 \\
&\overset{(a)}{\leq} -\gamma\nabla f\left(\boldsymbol{\theta}^t\right)^\top\left(\frac{1}{SK}\sum_{i\in\mathcal{S}_t,k}\frac{\boldsymbol{g}_i^{t,k}}{\left\|\boldsymbol{g}_i^{t,k}\right\|}\right) + \frac{\gamma^2 L}{2} \\
&= -\gamma\left(\nabla f\left(\boldsymbol{\theta}^t\right) - \boldsymbol{g}^t\right)^\top\left(\frac{1}{SK}\sum_{i\in\mathcal{S}_t,k}\frac{\boldsymbol{g}_i^{t,k}}{\left\|\boldsymbol{g}_i^{t,k}\right\|}\right) - \gamma\left(\boldsymbol{g}^t\right)^\top\left(\frac{1}{SK}\sum_{i\in\mathcal{S}_t,k}\frac{\boldsymbol{g}_i^{t,k}}{\left\|\boldsymbol{g}_i^{t,k}\right\|}\right) + \frac{\gamma^2 L}{2} \\
&\leq \gamma\left\|\nabla f\left(\boldsymbol{\theta}^t\right) - \boldsymbol{g}^t\right\| - \gamma\left(\boldsymbol{g}^t\right)^\top\left(\frac{1}{SK}\sum_{i\in\mathcal{S}_t,k}\frac{\boldsymbol{g}_i^{t,k}}{\left\|\boldsymbol{g}_i^{t,k}\right\|} - \frac{\boldsymbol{g}^t}{\|\boldsymbol{g}^t\|}\right) - \gamma\left\|\boldsymbol{g}^t\right\| + \frac{\gamma^2 L}{2} \\
&\overset{(b)}{\leq} 2\gamma\left\|\nabla f\left(\boldsymbol{\theta}^t\right) - \boldsymbol{g}^t\right\| - \gamma\left\|\nabla f\left(\boldsymbol{\theta}^t\right)\right\| + \gamma\left\|\boldsymbol{g}^t\right\|\left\|\frac{1}{SK}\sum_{i\in\mathcal{S}_t,k}\frac{\boldsymbol{g}_i^{t,k}}{\left\|\boldsymbol{g}_i^{t,k}\right\|} - \frac{\boldsymbol{g}^t}{\|\boldsymbol{g}^t\|}\right\| + \frac{\gamma^2 L}{2} \\
&\overset{(c)}{\leq} 2\gamma\left\|\nabla f\left(\boldsymbol{\theta}^t\right) - \boldsymbol{g}^t\right\| - \gamma\left\|\nabla f\left(\boldsymbol{\theta}^t\right)\right\| + \frac{\gamma}{SK}\sum_{i\in\mathcal{S}_t,k}\|\boldsymbol{g}_i^{t,k} - \boldsymbol{g}^t\| + \frac{\gamma^2 L}{2},
\end{aligned} \tag{A1}$$

where (a) uses the inequality that $\left\|\boldsymbol{\theta}^{t+1}-\boldsymbol{\theta}^{t}\right\| = \left\|\frac{\gamma}{SK}\sum_{i\in\mathcal{S}_t,k}\frac{\boldsymbol{g}_i^{t,k}}{\left\|\boldsymbol{g}_i^{t,k}\right\|}\right\| \leq \gamma$, (b) is based on $\gamma\left\|\nabla f\left(\boldsymbol{\theta}^{t}\right)\right\|-\gamma\left\|\boldsymbol{g}^{t}\right\| \leq \gamma\left\|\nabla f\left(\boldsymbol{\theta}^{t}\right)-\boldsymbol{g}^{t}\right\|$ and (c) is from the following relation:

$$\begin{aligned}
\left\|\boldsymbol{g}^{t}\right\|\left\|\frac{1}{SK}\sum_{i\in\mathcal{S}_t,k}\frac{\boldsymbol{g}_i^{t,k}}{\left\|\boldsymbol{g}_i^{t,k}\right\|}-\frac{\boldsymbol{g}^{t}}{\left\|\boldsymbol{g}^{t}\right\|}\right\| &= \frac{\left\|\boldsymbol{g}^{t}\right\|}{SK}\left\|\sum_{i\in\mathcal{S}_t,k}\left(\frac{\boldsymbol{g}_i^{t,k}}{\left\|\boldsymbol{g}_i^{t,k}\right\|}-\frac{\boldsymbol{g}_i^{t,k}}{\left\|\boldsymbol{g}^{t}\right\|}\right)\right\| \\
&= \frac{\left\|\boldsymbol{g}^{t}\right\|}{SK}\left\|\sum_{i\in\mathcal{S}_t,k}\frac{\left\|\boldsymbol{g}^{t}\right\|-\left\|\boldsymbol{g}_i^{t,k}\right\|}{\left\|\boldsymbol{g}^{t}\right\|\left\|\boldsymbol{g}_i^{t,k}\right\|}\boldsymbol{g}_i^{t,k}\right\| \\
&\leq \frac{\left\|\boldsymbol{g}^{t}\right\|}{SK}\sum_{i\in\mathcal{S}_t,k}\frac{\left|\left\|\boldsymbol{g}^{t}\right\|-\left\|\boldsymbol{g}_i^{t,k}\right\|\right|}{\left\|\boldsymbol{g}^{t}\right\|\left\|\boldsymbol{g}_i^{t,k}\right\|}\left\|\boldsymbol{g}_i^{t,k}\right\| \\
&= \frac{1}{SK}\sum_{i\in\mathcal{S}_t,k}\left|\left\|\boldsymbol{g}^{t}\right\|-\left\|\boldsymbol{g}_i^{t,k}\right\|\right| \\
&\leq \frac{1}{SK}\sum_{i\in\mathcal{S}_t,k}\left\|\boldsymbol{g}_i^{t,k}-\boldsymbol{g}^{t}\right\|.
\end{aligned}$$

Taking expectation on both sides of (A1), we obtain

$$\begin{aligned}
\gamma\mathbb{E}\left\|\nabla f\left(\boldsymbol{\theta}^{t}\right)\right\| \leq& \mathbb{E}\left[f\left(\boldsymbol{\theta}^{t}\right)-f\left(\boldsymbol{\theta}^{t+1}\right)\right]+2\gamma\mathbb{E}\left\|\nabla f\left(\boldsymbol{\theta}^{t}\right)-\boldsymbol{g}^{t}\right\| \\
&+\frac{\gamma}{SK}\mathbb{E}\left[\sum_{i\in\mathcal{S}_t,k}\left\|\boldsymbol{g}_i^{t,k}-\boldsymbol{g}^{t}\right\|\right]+\frac{\gamma^2 L}{2}.
\end{aligned}$$

Summing the above inequality over t and dividing it by γT, we have

$$\begin{aligned}
\frac{1}{T}\sum_{t=0}^{T-1}\mathbb{E}\left\|\nabla f\left(\boldsymbol{\theta}^{t}\right)\right\| \leq& \frac{1}{\gamma T}\mathbb{E}\left[f\left(\boldsymbol{\theta}^{0}\right)-f\left(\boldsymbol{\theta}^{T}\right)\right]+\frac{2}{T}\sum_{t=0}^{T-1}\mathbb{E}\left\|\nabla f\left(\boldsymbol{\theta}^{t}\right)-\boldsymbol{g}^{t}\right\| \\
&+\frac{1}{SKT}\sum_{t=0}^{T-1}\mathbb{E}\left[\sum_{i\in\mathcal{S}_t}\left\|\boldsymbol{g}_i^{t,k}-\boldsymbol{g}^{t}\right\|\right]+\frac{\gamma L}{2}. \qquad \text{(A2)}
\end{aligned}$$

We have the following results on the terms $\frac{1}{T}\sum_{t=0}^{T-1}\mathbb{E}\left\|\nabla f\left(\boldsymbol{\theta}^{t}\right)-\boldsymbol{g}^{t}\right\|$ and $\frac{1}{SKT}\sum_{t=0}^{T-1}\mathbb{E}\left[\sum_{i\in\mathcal{S}_t}\left\|\boldsymbol{g}_i^{t,k}-\boldsymbol{g}^{t}\right\|\right]$ in (A2).

Lemma 3. *Under Assumptions 2 and 3, the disparity $\frac{1}{T}\sum_{t=0}^{T-1}\mathbb{E}\left\|\nabla f\left(\boldsymbol{\theta}^{t}\right)-\boldsymbol{g}^{t}\right\|$ is upper bounded by:*

$$\begin{aligned}
\frac{1}{T}\sum_{t=0}^{T-1}\mathbb{E}\left\|\nabla f\left(\boldsymbol{\theta}^{t}\right)-\boldsymbol{g}^{t}\right\| \leq& \frac{1}{\beta T}\left(\frac{1}{2}\eta\beta KL+\frac{3\sigma}{\sqrt{SK}}\right)+\frac{\gamma L}{\beta}+\sqrt{1+\frac{10\beta}{S}}\eta KL+\sigma\sqrt{\frac{30\beta}{SK}} \\
&+2\gamma L\sqrt{\frac{\beta}{S}\left(1+\frac{4N^2}{S^2}\right)}+\sqrt{\frac{\eta\sqrt{K}L\sigma}{2\sqrt{S}}}.
\end{aligned}$$

Lemma 4. *Under Assumptions 2 and 3, the gradient dissimilarity $\frac{1}{SKT}\sum_{t=0}^{T-1}\mathbb{E}\left[\sum_{i\in\mathcal{S}_t}\left\|\boldsymbol{g}_i^{t,k}-\boldsymbol{g}^{t}\right\|\right]$ is upper bounded by:*

$$\begin{aligned}
\frac{1}{SKT}\sum_{t=1}^{T}\mathbb{E}\left[\sum_{i\in\mathcal{S}_t,k}\left\|\boldsymbol{g}_i^{t,k}-\boldsymbol{g}^{t}\right\|\right] \leq& 2\beta\left(\left(1+\frac{2}{\sqrt{K}}\right)\sigma+2\eta KL+\left(1+\frac{2N}{S}\right)\gamma L\right) \\
&+\frac{8N\beta}{ST}\left(\frac{\sqrt{2}\sigma}{\sqrt{K}}+\sqrt{\frac{2S}{3N}}\eta KL\right).
\end{aligned}$$

The proof of Lemma 3 is presented in subsection B.1 and the proof of Lemma 3 is presented in subsection B.2.

Set $\beta = \frac{\beta_0}{\sqrt{T}}$, $\gamma = \frac{\gamma_0}{T^{\frac{3}{4}}}$ and $\eta = \frac{1}{K\sqrt{T}}$. From Lemma 3, we know that

$$\begin{aligned}
&\frac{1}{T}\sum_{t=0}^{T-1}\mathbb{E}\left\|\nabla f\left(\boldsymbol{\theta}^t\right)-\boldsymbol{g}^t\right\| \\
&\leq \frac{1}{\beta_0\sqrt{T}}\left(\frac{\beta_0 L}{2T}+\frac{3\sigma}{\sqrt{SK}}\right)+\frac{\gamma_0 L}{\beta_0 T^{\frac{1}{4}}}+\sqrt{1+\frac{10\beta_0}{S\sqrt{T}}}\frac{L}{\sqrt{T}}+\sigma\sqrt{\frac{30\beta_0}{SK\sqrt{T}}} \\
&\quad+\frac{2\gamma_0 L}{T}\sqrt{\frac{\beta_0}{S}\left(1+\frac{4N^2}{S^2}\right)}+\sqrt{\frac{L\sigma}{2\sqrt{SKT}}} \\
&\lesssim \frac{3\sigma}{\beta_0\sqrt{SKT}}+\frac{\gamma_0 L}{\beta_0 T^{\frac{1}{4}}}+\frac{L}{\sqrt{T}}+\sigma\sqrt{\frac{30\beta_0}{SK\sqrt{T}}}+\sqrt{\frac{L\sigma}{2\sqrt{SKT}}}. \qquad \text{(A3)}
\end{aligned}$$

Similarly, from Lemma 4, we know that

$$\begin{aligned}
&\frac{1}{SKT}\sum_{t=0}^{T-1}\mathbb{E}\left[\sum_{i\in\mathcal{S}_t,k}\left\|\boldsymbol{g}_i^{t,k}-\boldsymbol{g}^t\right\|\right] \\
&\leq \frac{2\beta_0}{\sqrt{T}}\left(\left(1+\frac{2}{\sqrt{K}}\right)\sigma+\frac{2L}{\sqrt{T}}+\left(1+\frac{2N}{S}\right)\frac{\gamma_0 L}{T^{\frac{3}{4}}}\right)+\frac{8N\beta_0}{ST^{\frac{3}{2}}}\left(\frac{\sqrt{2}\sigma}{\sqrt{K}}+\sqrt{\frac{2S}{3N}}\frac{L}{\sqrt{T}}\right) \\
&\lesssim \frac{2\beta_0\sigma}{\sqrt{T}}+\frac{4\beta_0\sigma}{\sqrt{KT}}. \qquad \text{(A4)}
\end{aligned}$$

Define the initial optimality gap $\Delta := f\left(\boldsymbol{\theta}^0\right)-f^*$. Then, $f\left(\boldsymbol{\theta}^0\right)-f\left(\boldsymbol{\theta}^T\right)\leq f\left(\boldsymbol{\theta}^0\right)-f^*=\Delta$. Plugging (A3) and (A4) into (A2), we have

$$\begin{aligned}
\frac{1}{T}\sum_{t=0}^{T-1}\mathbb{E}\left\|\nabla f\left(\boldsymbol{\theta}^t\right)\right\| \lesssim & \frac{\Delta}{\gamma_0 T^{\frac{1}{4}}}+\frac{6\sigma}{\beta_0\sqrt{SKT}}+\frac{2\gamma_0 L}{\beta_0 T^{\frac{1}{4}}}+\frac{2L}{\sqrt{T}}+2\sigma\sqrt{\frac{30\beta_0}{SK\sqrt{T}}} \\
&+\frac{\sqrt{2L\sigma}}{(SKT)^{\frac{1}{4}}}+\frac{2\beta_0\sigma}{\sqrt{T}}+\frac{4\beta_0\sigma}{\sqrt{KT}}+\frac{\gamma_0 L}{2T^{\frac{3}{4}}}.
\end{aligned}$$

Let $\gamma_0=(SK)^{\frac{1}{4}}$ and $\beta_0=\sqrt{SK}$. Then, we have

$$\frac{1}{T}\sum_{t=0}^{T-1}\mathbb{E}\left\|\nabla f\left(\boldsymbol{\theta}^t\right)\right\| \leq \mathcal{O}\left(\frac{\Delta+L+\sigma+\sqrt{L\sigma}}{(SKT)^{\frac{1}{4}}}+\frac{\sqrt{SK}\sigma+L}{\sqrt{T}}\right).$$

By setting $SK\leq\mathcal{O}\left(T^{\frac{1}{3}}\right)$, we have $\frac{\sqrt{SK}}{\sqrt{T}}\propto\mathcal{O}\left((SKT)^{-\frac{1}{4}}\right)$ and thus

$$\frac{1}{T}\sum_{t=0}^{T-1}\mathbb{E}\left\|\nabla f\left(\boldsymbol{\theta}^t\right)\right\| \leq \mathcal{O}\left(\frac{\Delta+L+\sigma+\sqrt{L\sigma}}{(SKT)^{\frac{1}{4}}}\right).$$

B.1 Proof of Lemma 3

The proof of Lemma 3 utilizes the following result.

Lemma 5. *For any i,t, define $\boldsymbol{\phi}_i^t := \mathbb{E}\left\|\nabla f_i\left(\boldsymbol{\theta}^t\right)-\boldsymbol{c}_i^t\right\|^2$. Under Assumptions 2 and 3, we have*

$$\boldsymbol{\phi}_i^t \leq \left(\frac{2\sigma^2}{K}+\frac{2S}{3N}\eta^2K^2L^2\right)\left(1-\frac{S}{4N}\right)^{2t}+4\left(\frac{N^2}{S^2}\gamma^2L^2+\frac{\sigma^2}{K}+\frac{1}{3}\eta^2K^2L^2\right), \forall i.$$

Proof. Since for any t, the S elements in $\mathcal{S}_t$ are uniformly sampled from $\{1,\cdots,N\}$, we have

$$\boldsymbol{c}_i^t = \begin{cases} \boldsymbol{c}_i^{t-1} & \text{with probability} 1-\frac{S}{N} \\ \frac{1}{K}\sum_k \nabla F\left(\boldsymbol{\theta}_i^{t,k};\boldsymbol{\xi}_i^{t,k}\right) & \text{with probability} \frac{S}{N}. \end{cases}$$

Using Young's inequality repeatedly, we have

$$\begin{aligned}
\boldsymbol{\phi}_i^t =& \left(1-\frac{S}{N}\right)\mathbb{E}\left\|\nabla f_i\left(\boldsymbol{\theta}^t\right)-\boldsymbol{c}_i^{t-1}\right\|^2+\frac{S}{N}\mathbb{E}\left\|\frac{1}{K}\sum_k\left(\nabla f_i\left(\boldsymbol{\theta}^t\right)-\nabla F\left(\boldsymbol{\theta}_i^{t,k};\boldsymbol{\xi}_i^{t,k}\right)\right)\right\|^2 \\
\leq& \left(1-\frac{S}{N}\right)\mathbb{E}\left\|\nabla f_i\left(\boldsymbol{\theta}^t\right)\mp\nabla f_i\left(\boldsymbol{\theta}^{t-1}\right)-\boldsymbol{c}_i^{t-1}\right\|^2+\frac{S}{N}\left(\frac{2\sigma^2}{K}+\frac{2L^2}{K}\sum_k\mathbb{E}\left\|\boldsymbol{\theta}_i^{t,k}-\boldsymbol{\theta}^t\right\|^2\right) \\
\leq& \left(1-\frac{S}{N}\right)\mathbb{E}\left[\left(1+\frac{S}{2N}\right)\boldsymbol{\phi}_i^{t-1}+\left(1+\frac{2N}{S}\right)\gamma^2L^2\right]+\frac{2S}{N}\left(\frac{\sigma^2}{K}+\frac{1}{3}\eta^2K^2L^2\right) \\
\leq& \left(1-\frac{S}{2N}\right)\boldsymbol{\phi}_i^{t-1}+\frac{2N}{S}\gamma^2L^2+\frac{2S}{N}\left(\frac{\sigma^2}{K}+\frac{1}{3}\eta^2K^2L^2\right) \\
\leq& \left(1-\frac{S}{2N}\right)^t\boldsymbol{\phi}_i^0+\left(\frac{2N}{S}\gamma^2L^2+\frac{2S}{N}\left(\frac{\sigma^2}{K}+\frac{1}{3}\eta^2K^2L^2\right)\right)\sum_{\tau=0}^{t-1}\left(1-\frac{S}{2N}\right)^\tau \\
\leq& \left(1-\frac{S}{2N}\right)^t\boldsymbol{\phi}_i^0+4\left(\frac{N^2}{S^2}\gamma^2L^2+\frac{\sigma^2}{K}+\frac{1}{3}\eta^2K^2L^2\right).
\end{aligned}$$

Since $\boldsymbol{c}_i^{-1}=\frac{1}{K}\sum_{k=0}^{K-1}\nabla F\left(\boldsymbol{\theta}^0;\boldsymbol{\xi}_i^{-1,k}\right)$, we have

$$\begin{aligned}
\boldsymbol{\phi}_i^0 =& \left(1-\frac{S}{N}\right)\mathbb{E}\left\|\nabla f_i\left(\boldsymbol{\theta}^0\right)-\boldsymbol{c}_i^{-1}\right\|^2+\frac{S}{N}\mathbb{E}\left\|\nabla f_i\left(\boldsymbol{\theta}^0\right)-\frac{1}{K}\sum_k\nabla F\left(\boldsymbol{\theta}_i^{0,k};\boldsymbol{\xi}_i^{0,k}\right)\right\|^2 \\
\leq& \left(1-\frac{S}{N}\right)\frac{\sigma^2}{K}+\frac{2S}{N}\left(L^2\mathbb{E}\left\|\boldsymbol{\theta}^0-\boldsymbol{\theta}_i^{0,k}\right\|+\frac{\sigma^2}{K}\right) \\
\leq& \left(1+\frac{S}{N}\right)\frac{\sigma^2}{K}+\frac{2S}{3N}\eta^2K^2L^2 \\
\leq& \frac{2\sigma^2}{K}+\frac{2S}{3N}\eta^2K^2L^2.
\end{aligned}$$

Then, we have

$$\begin{aligned}
\boldsymbol{\phi}_i^t \leq& \left(\frac{2\sigma^2}{K}+\frac{2S}{3N}\eta^2K^2L^2\right)\left(1-\frac{S}{2N}\right)^t+4\left(\frac{N^2}{S^2}\gamma^2L^2+\frac{\sigma^2}{K}+\frac{1}{3}\eta^2K^2L^2\right) \\
\leq& \left(\frac{2\sigma^2}{K}+\frac{2S}{3N}\eta^2K^2L^2\right)\left(1-\frac{S}{4N}\right)^{2t}+4\left(\frac{N^2}{S^2}\gamma^2L^2+\frac{\sigma^2}{K}+\frac{1}{3}\eta^2K^2L^2\right),
\end{aligned}$$

where we use the relation $1-\frac{S}{2N}\leq\left(1-\frac{S}{4N}\right)^2$. □

Define $\mathcal{E}^t:=\nabla f\left(\boldsymbol{\theta}^t\right)-\boldsymbol{g}^t$ and $\boldsymbol{u}^t:=\nabla f\left(\boldsymbol{\theta}^t\right)-\nabla f\left(\boldsymbol{\theta}^{t-1}\right)$. From the update rule of momentum $\boldsymbol{g}^t$, we have

$$\begin{aligned}
\mathcal{E}^t =& (1-\beta)\left(\nabla f\left(\boldsymbol{\theta}^t\right)-\boldsymbol{g}^{t-1}\right)+\beta\underbrace{\left(\nabla f\left(\boldsymbol{\theta}^t\right)-\boldsymbol{c}^{t-1}-\frac{1}{SK}\sum_{i\in\mathcal{S}_t,k}\left(\nabla F\left(\boldsymbol{\theta}_i^{t,k};\boldsymbol{\xi}_i^{t,k}\right)-\boldsymbol{c}_i^{t-1}\right)\right)}_{:=\boldsymbol{v}^t} \\
=& (1-\beta)\mathcal{E}^{t-1}+(1-\beta)\boldsymbol{u}^t+\beta\boldsymbol{v}^t \\
=& (1-\beta)^t\mathcal{E}^0+\sum_{\tau=1}^t\boldsymbol{u}^\tau(1-\beta)^{t+1-\tau}+\sum_{\tau=1}^t\beta\boldsymbol{v}^\tau(1-\beta)^{t-\tau}.
\end{aligned}$$

Based on the triangle inequality of ℓ_2 norm and the concavity of the square root $(\cdot)^{\frac{1}{2}}$, we have

$$\mathbb{E}\left\|\mathcal{E}^t\right\|\leq(1-\beta)^t\mathbb{E}\left\|\mathcal{E}^0\right\|+\sum_{\tau=1}^t\mathbb{E}\left\|\boldsymbol{u}^\tau\right\|(1-\beta)^{t+1-\tau}+\left(\mathbb{E}\left\|\sum_{\tau=1}^t\beta\boldsymbol{v}^\tau(1-\beta)^{t-\tau}\right\|^2\right)^{\frac{1}{2}}. \quad \text{(A5)}$$

Since $\boldsymbol{c}_i^{-1} = \frac{1}{K}\sum_{k=0}^{K-1} \nabla F\left(\boldsymbol{\theta}^0; \boldsymbol{\xi}_i^{-1,k}\right)$ for any i, $\boldsymbol{c}^{-1} = \frac{1}{N}\sum_i \boldsymbol{c}_i^{-1}$, and $\boldsymbol{g}^{-1} = \boldsymbol{c}^{-1}$, we have

$$
\begin{aligned}
\mathbb{E}\left\|\mathcal{E}^0\right\| &= \mathbb{E}\left\|\nabla f\left(\boldsymbol{\theta}^0\right) - \frac{1}{NK}\sum_{i,k}\nabla F\left(\boldsymbol{\theta}^0; \boldsymbol{\xi}_i^{-1,k}\right) + \frac{\beta}{SK}\sum_{i\in\mathcal{S}_0,k}\left(\nabla F\left(\boldsymbol{\theta}_i^0; \boldsymbol{\xi}_i^{-1,k}\right) - \nabla F\left(\boldsymbol{\theta}_i^{0,k}; \boldsymbol{\xi}_i^{0,k}\right)\right)\right\| \\
&\leq \frac{\sigma}{\sqrt{NK}} + \mathbb{E}\left\|\frac{\beta}{SK}\sum_{i\in\mathcal{S}_0,k}\left(\nabla F\left(\boldsymbol{\theta}_i^0; \boldsymbol{\xi}_i^{-1,k}\right) \mp \nabla f_i\left(\boldsymbol{\theta}_i^0\right) \mp \nabla f_i\left(\boldsymbol{\theta}_i^{0,k}\right) - \nabla F\left(\boldsymbol{\theta}_i^{0,k}; \boldsymbol{\xi}_i^{0,k}\right)\right)\right\| \\
&\leq \frac{\sigma}{\sqrt{NK}} + \frac{\beta\sigma}{\sqrt{SK}} + \frac{\beta}{SK}\mathbb{E}\left[\sum_{i\in\mathcal{S}_0,k}\left\|\nabla f_i\left(\boldsymbol{\theta}^0\right) - \nabla f_i\left(\boldsymbol{\theta}_i^{0,k}\right)\right\|\right] + \frac{\beta\sigma}{\sqrt{SK}} \\
&\leq \frac{\beta L}{NK}\sum_{i,k}\mathbb{E}\left\|\boldsymbol{\theta}_i^{0,k} - \boldsymbol{\theta}^0\right\| + \frac{3\sigma}{\sqrt{SK}} \\
&\leq \frac{1}{2}\eta\beta KL + \frac{3\sigma}{\sqrt{SK}},
\end{aligned} \tag{A6}
$$

where the last inequality uses the results in Lemma 1.

Additionally, for any t, we have

$$
\left\|\boldsymbol{u}^t\right\| = \left\|\nabla f\left(\boldsymbol{\theta}^{t+1}\right) - \nabla f\left(\boldsymbol{\theta}^t\right)\right\| \leq L\left\|\boldsymbol{\theta}^{t+1} - \boldsymbol{\theta}^t\right\| \leq \gamma L\left\|\frac{1}{SK}\sum_{i\in\mathcal{S}_t,k}\frac{\boldsymbol{g}_i^{t,k}}{\|\boldsymbol{g}_i^{t,k}\|}\right\| \leq \gamma L. \tag{A7}
$$

To proceed, we handle the last term in (A5). First, we have

$$
\begin{aligned}
\mathbb{E}\left\|\sum_{\tau=1}^{t}\beta\boldsymbol{v}^\tau(1-\beta)^{t-\tau}\right\|^2 &= \sum_{\tau=1}^{t}\beta^2\mathbb{E}\|\boldsymbol{v}^\tau\|^2(1-\beta)^{2(t-\tau)} \\
&\quad + \sum_{1\leq\tau_1,\tau_2\leq t,\tau_1\neq\tau_2}\mathbb{E}\left\langle\beta\boldsymbol{v}^{\tau_1}(1-\beta)^{t-\tau_1}, \beta\boldsymbol{v}^{\tau_2}(1-\beta)^{t-\tau_2}\right\rangle.
\end{aligned} \tag{A8}
$$

Let $\mathcal{F}^0 \neq \emptyset$ and $\mathcal{F}_i^{t,k} := \sigma(\{\boldsymbol{\theta}_i^{t,j}\}_{0\leq j\leq k} \cup \mathcal{F}^t)$ and $\mathcal{F}^{t+1} := \sigma(\cup_i \mathcal{F}_i^{t,K})$ for all $t \geq 0$, where $\sigma()$ indicates the σ-algebra. Let $\mathbb{E}[\cdot|\mathcal{F}^t]$ represent the expectation conditioned on the filtration $\mathcal{F}^t$ with respect to the random variables $\{\boldsymbol{\xi}_i^{t,k}\}_{1\leq i\leq N, 0\leq k<K}$ in the t-th iteration. Let $\mathbb{E}_{\boldsymbol{\xi}_i^{t,k}}[\cdot]$ represent the expectation taking over the random sample $\boldsymbol{\xi}_i^{t,k}$. Similarly, let $\mathbb{E}_{\mathcal{S}_t}[\cdot]$ represent the expectation taking over the uniformly sampled client set $\mathcal{S}_t$. The set $\mathcal{S}_t$ is independent across different t. Then, for any t, we have

$$
\begin{aligned}
\mathbb{E}[\boldsymbol{v}^t|\mathcal{F}^t] &= \mathbb{E}_{\left\{\boldsymbol{\xi}_i^{t,k}\right\}_{\forall i,k},\mathcal{S}_t}[\boldsymbol{v}^t] \\
&= \mathbb{E}_{\left\{\boldsymbol{\xi}_i^{t,k}\right\}_{\forall i,k}}\left[\nabla f\left(\boldsymbol{\theta}^t\right) - \boldsymbol{c}^{t-1} - \frac{1}{NK}\sum_{i,k}\left(\nabla F\left(\boldsymbol{\theta}_i^{t,k}; \boldsymbol{\xi}_i^{t,k}\right) - \boldsymbol{c}_i^{t-1}\right)\right] \\
&= \nabla f\left(\boldsymbol{\theta}^t\right) - \frac{1}{NK}\sum_{i,k}\nabla f_i\left(\boldsymbol{\theta}_i^{t,k}\right),
\end{aligned}
$$

where the last equality is based on Assumption 3 and the fact that $\sum_{i=1}^{N} \boldsymbol{c}_i^t = \boldsymbol{c}^t$ for any t. Then, for any $0 \leq t_1 < t_2 \leq T-1$, we have

$$
\begin{aligned}
&\mathbb{E}\left\langle \boldsymbol{v}^{t_1}, \boldsymbol{v}^{t_2} \right\rangle \\
&= \mathbb{E}\left\langle \boldsymbol{v}^{t_1}, \mathbb{E}\left[\boldsymbol{v}^{t_2} | \mathcal{F}^{t_2}\right] \right\rangle \\
&= \mathbb{E}\left\langle \frac{1}{SK} \sum_{i \in \mathcal{S}_t, k} \left(\nabla f_i\left(\boldsymbol{\theta}^{t_1}\right) - \nabla f_i\left(\boldsymbol{\theta}_i^{t_1,k}\right) \right), \frac{1}{NK} \sum_{i,k} \left(\nabla f_i\left(\boldsymbol{\theta}^{t_2}\right) - \nabla f_i\left(\boldsymbol{\theta}_i^{t_2,k}\right) \right) \right\rangle \\
&+ \mathbb{E}\left\langle \frac{1}{SK} \sum_{i \in \mathcal{S}_t, k} \left(\nabla f_i\left(\boldsymbol{\theta}_i^{t_1,k}\right) - \nabla F\left(\boldsymbol{\theta}_i^{t_1,k}; \boldsymbol{\xi}_i^{t_1,k}\right) \right), \frac{1}{NK} \sum_{i,k} \left(\nabla f_i\left(\boldsymbol{\theta}^{t_2}\right) - \nabla f_i\left(\boldsymbol{\theta}_i^{t_2,k}\right) \right) \right\rangle \\
&+ \mathbb{E}\left\langle \mathbb{E}_{\mathcal{S}_t}\left[\frac{1}{S} \sum_{i \in \mathcal{S}_t} \boldsymbol{c}^{t-1} - \boldsymbol{c}_i^{t-1} \right], \frac{1}{NK} \sum_{i,k} \left(\nabla f_i\left(\boldsymbol{\theta}^{t_2}\right) - \nabla f_i\left(\boldsymbol{\theta}_i^{t_2,k}\right) \right) \right\rangle \\
&\leq \frac{L^2}{2NK} \sum_{i,k} \mathbb{E}\left\| \boldsymbol{\theta}_i^{t_1,k} - \boldsymbol{\theta}^{t_1} \right\|^2 + \frac{L^2}{2NK} \sum_{i,k} \mathbb{E}\left\| \boldsymbol{\theta}_i^{t_2,k} - \boldsymbol{\theta}^{t_2} \right\|^2 + \frac{\sigma}{\sqrt{SK}} \frac{L}{NK} \sum_{i,k} \left\| \boldsymbol{\theta}_i^{t_2,k} - \boldsymbol{\theta}^{t_2} \right\| \\
&\leq \frac{1}{3}\eta^2 K^2 L^2 + \frac{\eta\sqrt{K} L \sigma}{2\sqrt{S}}.
\end{aligned} \tag{A9}
$$

Further, based on Lemma 2, we have

$$
\begin{aligned}
\mathbb{E}\left\|\boldsymbol{v}^t\right\|^2 \leq & \mathbb{E}\left\| \nabla f\left(\boldsymbol{\theta}^t\right) - \frac{1}{NK} \sum_{i,k} \nabla F\left(\boldsymbol{\theta}_i^{t,k}; \boldsymbol{\xi}_i^{t,k}\right) \right\|^2 \\
& + \frac{1}{S} \underbrace{\frac{1}{N} \sum_i \mathbb{E}\left\| \frac{1}{K} \sum_k \left(\nabla F\left(\boldsymbol{\theta}_i^{t,k}; \boldsymbol{\xi}_i^{t,k}\right) - \frac{1}{N} \sum_i \nabla F\left(\boldsymbol{\theta}_i^{t,k}; \boldsymbol{\xi}_i^{t,k}\right) \right) - \left(\boldsymbol{c}_i^{t-1} - \boldsymbol{c}^{t-1}\right) \right\|^2}_{:=\Lambda_t} \\
\leq & 2\left(L^2 \mathbb{E}\left\| \boldsymbol{\theta}^t - \boldsymbol{\theta}_i^{t,k} \right\| + \frac{\sigma^2}{NK} \right) + \frac{\Lambda_t}{S} \\
\leq & \frac{2}{3}\eta^2 K^2 L^2 + \frac{2\sigma^2}{NK} + \frac{\Lambda_t}{S}.
\end{aligned}
$$

$$
\begin{aligned}
\Lambda_t &\leq \frac{1}{N} \sum_i \mathbb{E}\left\| \frac{1}{K} \sum_k \nabla F\left(\boldsymbol{\theta}_i^{t,k}; \boldsymbol{\xi}_i^{t,k}\right) - \boldsymbol{c}_i^{t-1} \right\|^2 \\
&= \frac{1}{N} \sum_i \mathbb{E}\left\| \frac{1}{K} \sum_k \nabla F\left(\boldsymbol{\theta}_i^{t,k}; \boldsymbol{\xi}_i^{t,k}\right) \mp \nabla f_i\left(\boldsymbol{\theta}_i^{t,k}\right) \mp \nabla f_i\left(\boldsymbol{\theta}^t\right) \mp \nabla f_i\left(\boldsymbol{\theta}^{t-1}\right) - \boldsymbol{c}_i^{t-1} \right\|^2 \\
&\leq \frac{4\sigma^2}{K} + \frac{4L^2}{NK} \sum_{i,k} \mathbb{E}\left\| \boldsymbol{\theta}_i^{t,k} - \boldsymbol{\theta}^t \right\|^2 + 4L^2 \mathbb{E}\left\| \boldsymbol{\theta}^t - \boldsymbol{\theta}^{t-1} \right\|^2 + \frac{4}{N} \sum_i \mathbb{E}\left\| \nabla f_i\left(\boldsymbol{\theta}^{t-1}\right) - \boldsymbol{c}_i^{t-1} \right\|^2 \\
&\leq \frac{4\sigma^2}{K} + \frac{4}{3}\eta^2 K^2 L^2 + 4\gamma^2 L^2 + \frac{4}{N} \sum_i \boldsymbol{\phi}_i^{t-1},
\end{aligned}
$$

where $\boldsymbol{\phi}_i^{t-1} := \mathbb{E}\left\| \nabla f_i\left(\boldsymbol{\theta}^{t-1}\right) - \boldsymbol{c}_i^{t-1} \right\|^2$. From Lemma 5, we know that, for any i,

$$
\begin{aligned}
\boldsymbol{\phi}_i^{t-1} &\leq \left(\frac{2\sigma^2}{K} + \frac{2S}{3N}\eta^2 K^2 L^2 \right) \left(1 - \frac{S}{4N} \right)^{2(t-1)} + 4\left(\frac{N^2}{S^2}\gamma^2 L^2 + \frac{\sigma^2}{K} + \frac{1}{3}\eta^2 K^2 L^2 \right) \\
&\leq \frac{6\sigma^2}{K} + 2\eta^2 K^2 L^2 + \frac{4N^2}{S^2}\gamma^2 L^2.
\end{aligned} \tag{A10}
$$

Plugging the upper bound of $\boldsymbol{\phi}_i^{t-1}$ into Λ_t yields

$$
\Lambda_t \leq \frac{28\sigma^2}{K} + \frac{28}{3}\eta^2 K^2 L^2 + 4\gamma^2 L^2 \left(1 + \frac{4N^2}{S^2} \right).
$$

Then, we have

$$\mathbb{E}\left\|\boldsymbol{v}^t\right\|^2 \leq \left(\frac{2}{3}+\frac{10}{S}\right)\eta^2K^2L^2+\frac{30\sigma^2}{SK}+\frac{4\gamma^2L^2}{S}\left(1+\frac{4N^2}{S^2}\right). \tag{A11}$$

Plugging (A9) and (A11) into (A8) gives

$$\begin{aligned}\mathbb{E}\left\|\sum_{\tau=1}^{t}\beta\boldsymbol{v}^\tau(1-\beta)^{t-\tau}\right\|^2 \leq& \beta\mathbb{E}\|\boldsymbol{v}^\tau\|^2+\mathbb{E}\left\langle\boldsymbol{v}^{\tau_1},\boldsymbol{v}^{\tau_2}\right\rangle\\ \leq& \left(\frac{2}{3}+\frac{10}{S}\right)\beta\eta^2K^2L^2+\frac{30\sigma^2\beta}{SK}+\frac{4\beta\gamma^2L^2}{S}\left(1+\frac{4N^2}{S^2}\right)\\ &+\frac{1}{3}\eta^2K^2L^2+\frac{\eta\sqrt{K}L\sigma}{2\sqrt{S}}.\end{aligned}$$

Since $\beta\leq 1$, taking square root on both sides of the above inequality yields

$$\begin{aligned}&\left(\mathbb{E}\left\|\sum_{\tau=1}^{t}\beta\boldsymbol{v}^\tau(1-\beta)^{t-\tau}\right\|^2\right)^{\frac{1}{2}}\\ &\leq\sqrt{1+\frac{10\beta}{S}}\eta KL+\sigma\sqrt{\frac{30\beta}{SK}}+2\gamma L\sqrt{\frac{\beta}{S}\left(1+\frac{4N^2}{S^2}\right)}+\sqrt{\frac{\eta\sqrt{K}L\sigma}{2\sqrt{S}}},\end{aligned} \tag{A12}$$

where we use the fact that $\sqrt{a+b}\leq\sqrt{a}+\sqrt{b}$, for any $a,b\geq 0$.

Plugging (A6), (A7), and (A12) into (A5), we have

$$\begin{aligned}\mathbb{E}\|\mathcal{E}^t\| \leq&(1-\beta)^t\left(\frac{1}{2}\eta\beta KL+\frac{3\sigma}{\sqrt{SK}}\right)+\frac{\gamma L}{\beta}+\sqrt{1+\frac{10\beta}{S}}\eta KL+\sigma\sqrt{\frac{30\beta}{SK}}\\ &+2\gamma L\sqrt{\frac{\beta}{S}\left(1+\frac{4N^2}{S^2}\right)}+\sqrt{\frac{\eta\sqrt{K}L\sigma}{2\sqrt{S}}}.\end{aligned}$$

Summing the above inequality over t yields

$$\begin{aligned}\frac{1}{T}\sum_{t=0}^{T-1}\mathbb{E}\|\mathcal{E}^t\| \leq&\frac{1}{\beta T}\left(\frac{1}{2}\eta\beta KL+\frac{3\sigma}{\sqrt{SK}}\right)+\frac{\gamma L}{\beta}+\sqrt{1+\frac{10\beta}{S}}\eta KL+\sigma\sqrt{\frac{30\beta}{SK}}\\ &+2\gamma L\sqrt{\frac{\beta}{S}\left(1+\frac{4N^2}{S^2}\right)}+\sqrt{\frac{\eta\sqrt{K}L\sigma}{2\sqrt{S}}}.\end{aligned}$$

B.2 Proof of Lemma 4

Recall that $\boldsymbol{g}_i^{t,k}=\beta\left(\nabla F\left(\boldsymbol{\theta}_i^{t,k};\boldsymbol{\xi}_i^{t,k}\right)-\boldsymbol{c}_i^{t-1}+\boldsymbol{c}^{t-1}\right)+(1-\beta)\boldsymbol{g}^{t-1}$, and

$$\begin{aligned}\boldsymbol{g}^t=&\frac{1}{SK}\sum_{i\in\mathcal{S}_t,k}\boldsymbol{g}_i^{t,k}\\ =&\beta\left(\frac{1}{S}\sum_{i\in\mathcal{S}_t}\left(\frac{1}{K}\sum_{k=0}^{K-1}\nabla F\left(\boldsymbol{\theta}_i^{t,k};\boldsymbol{\xi}_i^{t,k}\right)-\boldsymbol{c}_i^{t-1}\right)+\boldsymbol{c}^{t-1}\right)+(1-\beta)\boldsymbol{g}^{t-1}.\end{aligned}$$

Then, we have

$$
\begin{aligned}
&\mathbb{E}\left[\frac{1}{SK}\sum_{i\in\mathcal{S}_t,k}\left\|\boldsymbol{g}_i^{t,k}-\boldsymbol{g}^t\right\|\right]\\
&=\beta\mathbb{E}\left[\frac{1}{SK}\sum_{i\in\mathcal{S}_t,k}\left\|\nabla F\left(\boldsymbol{\theta}_i^{t,k};\boldsymbol{\xi}_i^{t,k}\right)-\boldsymbol{c}_i^{t-1}-\frac{1}{S}\sum_{i\in\mathcal{S}_t}\left(\frac{1}{K}\sum_{k=0}^{K-1}\nabla F\left(\boldsymbol{\theta}_i^{t,k};\boldsymbol{\xi}_i^{t,k}\right)-\boldsymbol{c}_i^{t-1}\right)\right\|\right]\\
&\leq\frac{2\beta}{NK}\sum_{i,k}\mathbb{E}\left\|\nabla F\left(\boldsymbol{\theta}_i^{t,k};\boldsymbol{\xi}_i^{t,k}\right)-\boldsymbol{c}_i^{t-1}\right\|\\
&=\frac{2\beta}{NK}\sum_{i,k}\mathbb{E}\left\|\nabla F\left(\boldsymbol{\theta}_i^{t,k};\boldsymbol{\xi}_i^{t,k}\right)\mp\nabla f_i\left(\boldsymbol{\theta}_i^{t,k}\right)\mp\nabla f_i\left(\boldsymbol{\theta}^t\right)\mp\nabla f_i\left(\boldsymbol{\theta}^{t-1}\right)-\boldsymbol{c}_i^{t-1}\right\|\\
&\leq 2\beta\left(\sigma+\frac{L}{NK}\sum_{i,k}\left\|\boldsymbol{\theta}_i^{t,k}-\boldsymbol{\theta}^t\right\|+L\left\|\boldsymbol{\theta}^t-\boldsymbol{\theta}^{t-1}\right\|\right)+\frac{2\beta}{N}\sum_i\mathbb{E}\left\|\nabla f_i\left(\boldsymbol{\theta}^{t-1}\right)-\boldsymbol{c}_i^{t-1}\right\|\\
&\leq 2\beta\left(\sigma+\frac{1}{2}\eta KL+\gamma L\right)+\frac{2\beta}{N}\sum_i\sqrt{\boldsymbol{\phi}_i^{t-1}}.
\end{aligned}
$$

From Lemma 5, we know that

$$
\sqrt{\boldsymbol{\phi}_i^{t-1}}\leq\left(\frac{\sqrt{2}\sigma}{\sqrt{K}}+\sqrt{\frac{2S}{3N}}\eta KL\right)\left(1-\frac{S}{4N}\right)^{t-1}+2\left(\frac{N}{S}\gamma L+\frac{\sigma}{\sqrt{K}}+\frac{1}{\sqrt{3}}\eta KL\right),\forall i.
$$

Thus, we have

$$
\begin{aligned}
\mathbb{E}\left[\frac{1}{SK}\sum_{i\in\mathcal{S}_t,k}\left\|\boldsymbol{g}_i^{t,k}-\boldsymbol{g}^t\right\|\right]\leq&2\beta\left(\left(1+\frac{2}{\sqrt{K}}\right)\sigma+2\eta KL+\left(1+\frac{2N}{S}\right)\gamma L\right)\\
&+2\beta\left(\frac{\sqrt{2}\sigma}{\sqrt{K}}+\sqrt{\frac{2S}{3N}}\eta KL\right)\left(1-\frac{S}{4N}\right)^{t-1}.
\end{aligned}
$$

Summing the above inequality over t yields

$$
\begin{aligned}
\frac{1}{SKT}\sum_{t=1}^{T}\mathbb{E}\left[\sum_{i\in\mathcal{S}_t,k}\left\|\boldsymbol{g}_i^{t,k}-\boldsymbol{g}^t\right\|\right]\leq&2\beta\left(\left(1+\frac{2}{\sqrt{K}}\right)\sigma+2\eta KL+\left(1+\frac{2N}{S}\right)\gamma L\right)\\
&+\frac{8N\beta}{ST}\left(\frac{\sqrt{2}\sigma}{\sqrt{K}}+\sqrt{\frac{2S}{3N}}\eta KL\right).
\end{aligned}
$$

C Theoretical Analysis of PAdaMFed with Variance Reduction

The analysis of PAdaMFed-VR is similar to that of PAdaMFed. We first present the following two auxiliary Lemmas.

Lemma 6. *Under Assumptions 1 and 3, the disparity* $\frac{1}{T}\sum_{t=0}^{T-1}\mathbb{E}\left\|\nabla f\left(\boldsymbol{\theta}^t\right)-\boldsymbol{g}^t\right\|$ *is upper bounded by:*

$$
\begin{aligned}
\frac{1}{T}\sum_{t=0}^{T-1}\mathbb{E}\left\|\nabla f\left(\boldsymbol{\theta}^t\right)-\boldsymbol{g}^t\right\|\leq&\frac{1}{\beta T}\left(\frac{1}{2}\eta KL+\frac{3\sigma}{\sqrt{SK}}\right)+\frac{\eta KL}{2\beta}+\gamma L\sqrt{\frac{2}{SK\beta}}+\sigma\sqrt{\frac{22\beta}{SK}}\\
&+\gamma L\sqrt{\frac{3\beta}{S}\left(1+\frac{4N^2}{S^2}\right)}+\eta KL\sqrt{\frac{6\beta}{S}}.
\end{aligned}
$$

Algorithm 2 PAdaMFed-VR: PAdaMFed with Variance Reduction

Require: initial model $\boldsymbol{\theta}^0$, $\boldsymbol{\theta}^{-1} = \boldsymbol{\theta}^0$, control variates $\boldsymbol{c}_i^{-1} = \frac{1}{K}\sum_{k=0}^{K-1} \nabla F\left(\boldsymbol{\theta}^0; \boldsymbol{\xi}_i^{-1,k}\right)$ for any i, $\boldsymbol{c}^{-1} = \frac{1}{N}\sum_i \boldsymbol{c}_i^{-1}$, momentum $\boldsymbol{g}^{-1} = \boldsymbol{c}^{-1}$, global learning rate γ, local learning rate η, and momentum parameter β
for $t = 0, \cdots, T-1$ **do**
  Central Server: Uniformly sample clients $\mathcal{S}_t \subseteq \{1, \cdots, N\}$ with $|\mathcal{S}_t| = S$
  for each client $i \in \mathcal{S}_t$ in parallel **do**
    Initialize local model $\boldsymbol{\theta}_i^{t,0} = \boldsymbol{\theta}^t$ and control variate $\boldsymbol{c}_i^t = \mathbf{0}$ (for $i \notin \mathcal{S}_t$, $\boldsymbol{c}_i^t = \boldsymbol{c}_i^{t-1}$)
    for $k = 0, \cdots, K-1$ **do**
      Compute $\boldsymbol{g}_i^{t,k} = \nabla F\left(\boldsymbol{\theta}_i^{t,k}; \boldsymbol{\xi}_i^{t,k}\right) + \beta\left(\boldsymbol{c}^{t-1} - \boldsymbol{c}_i^{t-1}\right) + (1-\beta)\left(\boldsymbol{g}^{t-1} - \nabla F\left(\boldsymbol{\theta}^{t-1}; \boldsymbol{\xi}_i^{t,k}\right)\right)$
      Update local model $\boldsymbol{\theta}_i^{t,k+1} = \boldsymbol{\theta}_i^{t,k} - \eta \frac{\boldsymbol{g}_i^{t,k}}{\|\boldsymbol{g}_i^{t,k}\|}$
      Update control variate $\boldsymbol{c}_i^t = \boldsymbol{c}_i^t + \frac{1}{K}\nabla F\left(\boldsymbol{\theta}_i^{t,k}; \boldsymbol{\xi}_i^{t,k}\right)$
    end for
    Upload $\boldsymbol{\theta}_i^{t,K}$ and $\boldsymbol{c}_i^t$ to central server
  end for
  Central server:
  Aggregate local updates $\overline{\boldsymbol{g}}^t = \frac{1}{\eta SK}\sum_{i\in\mathcal{S}_t}\left(\boldsymbol{\theta}^t - \boldsymbol{\theta}_i^{t,K}\right)$
  Update global model $\boldsymbol{\theta}^{t+1} = \boldsymbol{\theta}^t - \gamma\overline{\boldsymbol{g}}^t$
  Aggregate control variate $\boldsymbol{c}^t = \boldsymbol{c}^{t-1} + \frac{1}{N}\sum_{i\in\mathcal{S}_t}\left(\boldsymbol{c}_i^t - \boldsymbol{c}_i^{t-1}\right)$
  Aggregate momentum $\boldsymbol{g}^t = \beta\left(\frac{1}{S}\sum_{i\in\mathcal{S}_t}\left(\boldsymbol{c}_i^t - \boldsymbol{c}_i^{t-1}\right) + \boldsymbol{c}^{t-1}\right) + (1-\beta)\boldsymbol{g}^{t-1}$
  Download $\boldsymbol{\theta}^{t+1}$, $\boldsymbol{c}^t$, and $\boldsymbol{g}^t$ to all clients
end for

Lemma 7. *Under Assumptions 1 and 3, the gradient dissimilarity* $\frac{1}{SKT}\sum_{t=0}^{T-1}\mathbb{E}\left[\sum_{i\in\mathcal{S}_t}\left\|\boldsymbol{g}_i^{t,k} - \boldsymbol{g}^t\right\|\right]$ *is upper bounded by:*

$$\frac{1}{SKT}\sum_{t=1}^{T}\mathbb{E}\left[\sum_{i\in\mathcal{S}_t,k}\left\|\boldsymbol{g}_i^{t,k} - \boldsymbol{g}^t\right\|\right] \leq 2\beta\left(\left(1+\frac{2}{\sqrt{K}}\right)\sigma + 2\eta KL + \left(1+\frac{2N}{S}\right)\gamma L\right) + \frac{8N\beta}{ST}\left(\frac{\sqrt{2}\sigma}{\sqrt{K}} + \sqrt{\frac{2S}{3N}}\eta KL\right) + \eta KL + 2\gamma L.$$

Set $\beta = \frac{\beta_0}{T^{\frac{2}{3}}}$ and $\gamma = \frac{\gamma_0}{T^{\frac{2}{3}}}$. $\eta = \frac{1}{KT}$. From Lemma 6, we know that

$$\begin{aligned}\frac{1}{T}\sum_{t=0}^{T-1}\mathbb{E}\left\|\nabla f\left(\boldsymbol{\theta}^t\right) - \boldsymbol{g}^t\right\| \leq& \frac{1}{\beta_0 T^{\frac{1}{3}}}\left(\frac{L}{2T} + \frac{3\sigma}{\sqrt{SK}}\right) + \frac{L}{2\beta_0 T^{\frac{1}{3}}} + \frac{\gamma_0 L}{T^{\frac{1}{3}}}\sqrt{\frac{2}{SK\beta_0}} + \frac{\sigma}{T^{\frac{1}{3}}}\sqrt{\frac{22\beta_0}{SK}} \\ &+ \frac{\gamma_0 L}{T}\sqrt{\frac{3\beta_0}{S}\left(1+\frac{4N^2}{S^2}\right)} + \frac{L}{T^{\frac{4}{3}}}\sqrt{\frac{6\beta_0}{S}} \\ \lesssim& \frac{3\sigma}{\beta_0\sqrt{SK}T^{\frac{1}{3}}} + \frac{L}{2\beta_0 T^{\frac{1}{3}}} + \frac{\gamma_0 L}{T^{\frac{1}{3}}}\sqrt{\frac{2}{SK\beta_0}} + \frac{\sigma}{T^{\frac{1}{3}}}\sqrt{\frac{22\beta_0}{SK}}. \end{aligned} \tag{A13}$$

Similarly, from Lemma 7, we have

$$\begin{aligned}\frac{1}{SKT}\sum_{t=1}^{T}\mathbb{E}\left[\sum_{i\in\mathcal{S}_t,k}\left\|\boldsymbol{g}_i^{t,k} - \boldsymbol{g}^t\right\|\right] \leq& \frac{2\beta_0}{T^{\frac{2}{3}}}\left(\left(1+\frac{2}{\sqrt{K}}\right)\sigma + \frac{2L}{T} + \left(1+\frac{2N}{S}\right)\frac{\gamma_0 L}{T^{\frac{2}{3}}}\right) \\ &+ \frac{8N\beta_0}{ST^{\frac{5}{3}}}\left(\frac{\sqrt{2}\sigma}{\sqrt{K}} + \sqrt{\frac{2S}{3N}}\frac{L}{T}\right) + \frac{L}{T} + \frac{2\gamma_0 L}{T^{\frac{2}{3}}}. \end{aligned} \tag{A14}$$

Plugging (A13) and (A14) into (A2), we have

$$\frac{1}{T}\sum_{t=0}^{T-1}\mathbb{E}\left\|\nabla f\left(\boldsymbol{\theta}^t\right)\right\| \lesssim \frac{\Delta}{\gamma_0 T^{\frac{1}{3}}}+\frac{6\sigma}{\beta_0\sqrt{SK}T^{\frac{1}{3}}}+\frac{L}{\beta_0 T^{\frac{1}{3}}}+\frac{2\sqrt{2}\gamma_0 L}{\sqrt{SK\beta_0}T^{\frac{1}{3}}}+\frac{2\sigma\sqrt{22\beta_0}}{\sqrt{SK}T^{\frac{1}{3}}} + \frac{2\beta_0\sigma}{T^{\frac{2}{3}}}+\frac{2\gamma_0 L}{T^{\frac{2}{3}}}.$$

Set $\beta_0=(SK)^{\frac{1}{3}}$ and $\gamma_0=(SK)^{\frac{1}{3}}$, we have

$$\begin{aligned}\frac{1}{T}\sum_{t=0}^{T-1}\mathbb{E}\left\|\nabla f\left(\boldsymbol{\theta}^t\right)\right\| \lesssim & \frac{\Delta}{\gamma_0 T^{\frac{1}{3}}}+\frac{6\sigma}{\beta_0\sqrt{SK}T^{\frac{1}{3}}}+\frac{L}{\beta_0 T^{\frac{1}{3}}}+\frac{2\sqrt{2}\gamma_0 L}{\sqrt{SK\beta_0}T^{\frac{1}{3}}} \\ & + \frac{2\sigma\sqrt{22\beta_0}}{\sqrt{SK}T^{\frac{1}{3}}}+\frac{2\beta_0\sigma}{T^{\frac{2}{3}}}+\frac{2\gamma_0 L}{T^{\frac{2}{3}}} \\ \leq & \mathcal{O}\left(\frac{\Delta+L+\sigma}{(SKT)^{\frac{1}{3}}}+\frac{(L+\sigma)(SK)^{\frac{1}{3}}}{T^{\frac{2}{3}}}\right).\end{aligned}$$

By setting $SK\leq\mathcal{O}\left(\sqrt{T}\right)$, we have $\frac{(SK)^{\frac{1}{3}}}{T^{\frac{2}{3}}}\propto\mathcal{O}\left((SKT)^{-\frac{1}{3}}\right)$ and thus

$$\frac{1}{T}\sum_{t=0}^{T-1}\mathbb{E}\left\|\nabla f\left(\boldsymbol{\theta}^t\right)\right\| \leq \mathcal{O}\left(\frac{\Delta+L+\sigma}{(SKT)^{\frac{1}{3}}}\right).$$

C.1 Proof of Lemma 6

Since $\mathcal{E}^t:=\nabla f\left(\boldsymbol{\theta}^t\right)-\boldsymbol{g}^t$, we have

$$\begin{aligned}\mathcal{E}^t =& \nabla f\left(\boldsymbol{\theta}^t\right)-\frac{1}{SK}\sum_{i\in\mathcal{S}_t,k}\nabla F\left(\boldsymbol{\theta}_i^{t,k};\boldsymbol{\xi}_i^{t,k}\right)+\frac{\beta}{S}\sum_{i\in\mathcal{S}_t}\left(\boldsymbol{c}_i^{t-1}-\boldsymbol{c}^{t-1}\right) \\ & -(1-\beta)\left(\boldsymbol{g}^{t-1}\mp\nabla f\left(\boldsymbol{\theta}^{t-1}\right)-\frac{1}{SK}\sum_{i\in\mathcal{S}_t,k}\nabla F\left(\boldsymbol{\theta}^{t-1};\boldsymbol{\xi}_i^{t,k}\right)\right) \\ =&(1-\beta)\mathcal{E}^{t-1}+\underbrace{\frac{1}{SK}\sum_{i\in\mathcal{S}_t,k}\left(\nabla F\left(\boldsymbol{\theta}^t;\boldsymbol{\xi}_i^{t,k}\right)-\nabla F\left(\boldsymbol{\theta}_i^{t,k};\boldsymbol{\xi}_i^{t,k}\right)\right)}_{:=\boldsymbol{w}^t} \\ & +\beta\underbrace{\left(\nabla f\left(\boldsymbol{\theta}^t\right)-\boldsymbol{c}^{t-1}-\frac{1}{SK}\sum_{i\in\mathcal{S}_t,k}\left(\nabla F\left(\boldsymbol{\theta}^t;\boldsymbol{\xi}_i^{t,k}\right)-\boldsymbol{c}_i^{t-1}\right)\right)}_{:=\widetilde{\boldsymbol{v}}^t} \\ & +(1-\beta)\underbrace{\left(\frac{1}{SK}\sum_{i\in\mathcal{S}_t,k}\left(\nabla F\left(\boldsymbol{\theta}^{t-1};\boldsymbol{\xi}_i^{t,k}\right)-\nabla F\left(\boldsymbol{\theta}^t;\boldsymbol{\xi}_i^{t,k}\right)\right)+\nabla f\left(\boldsymbol{\theta}^t\right)-\nabla f\left(\boldsymbol{\theta}^{t-1}\right)\right)}_{:=\widetilde{\boldsymbol{u}}^t} \\ =&(1-\beta)^t\mathcal{E}^0+\sum_{\tau=1}^t\boldsymbol{w}^\tau(1-\beta)^{t-\tau}+\sum_{\tau=1}^t\widetilde{\boldsymbol{u}}^\tau(1-\beta)^{t+1-\tau}+\sum_{\tau=1}^t\beta\widetilde{\boldsymbol{v}}^\tau(1-\beta)^{t-\tau}.\end{aligned}$$

$$\begin{aligned}\mathbb{E}\left\|\mathcal{E}^t\right\| \leq & (1-\beta)^t\mathbb{E}\left\|\mathcal{E}^0\right\|+\sum_{\tau=1}^t\mathbb{E}\left\|\boldsymbol{w}^t\right\|(1-\beta)^{t-\tau}+\left(\mathbb{E}\left\|\sum_{\tau=1}^t\widetilde{\boldsymbol{u}}^\tau(1-\beta)^{t+1-\tau}\right\|^2\right)^{\frac{1}{2}} \\ & +\left(\mathbb{E}\left\|\sum_{\tau=1}^t\beta\widetilde{\boldsymbol{v}}^\tau(1-\beta)^{t-\tau}\right\|^2\right)^{\frac{1}{2}}. \qquad \text{(A15)}\end{aligned}$$

Since $\boldsymbol{\theta}^{-1} = \boldsymbol{\theta}^0$, $\boldsymbol{c}_i^{-1} = \frac{1}{K}\sum_{k=0}^{K-1} \nabla F\left(\boldsymbol{\theta}^0; \boldsymbol{\xi}_i^{-1,k}\right)$ for any i, $\boldsymbol{c}^{-1} = \frac{1}{N}\sum_i \boldsymbol{c}_i^{-1}$, and $\boldsymbol{g}^{-1} = \boldsymbol{c}^{-1}$, we have

$$\begin{aligned}
\mathbb{E}\left\|\mathcal{E}^0\right\| =& \mathbb{E}\Bigg\|\nabla f\left(\boldsymbol{\theta}^0\right) - \frac{1}{NK}\sum_{i,k}\nabla F\left(\boldsymbol{\theta}^0; \boldsymbol{\xi}_i^{-1,k}\right) \\
&+ \frac{1}{SK}\sum_{i\in\mathcal{S}_0,k}\left(\beta\nabla F\left(\boldsymbol{\theta}_i^0; \boldsymbol{\xi}_i^{-1,k}\right) + (1-\beta)\nabla F\left(\boldsymbol{\theta}^0; \boldsymbol{\xi}_i^{0,k}\right) - \nabla F\left(\boldsymbol{\theta}_i^{0,k}; \boldsymbol{\xi}_i^{0,k}\right)\right)\Bigg\| \\
\leq& \frac{\sigma}{\sqrt{NK}} + \frac{\sigma}{\sqrt{SK}} + \frac{1}{SK}\mathbb{E}\left[\sum_{i\in\mathcal{S}_0,k}\left\|\nabla f_i\left(\boldsymbol{\theta}^0\right) - \nabla f_i\left(\boldsymbol{\theta}_i^{0,k}\right)\right\|\right] + \frac{\sigma}{\sqrt{SK}} \\
\leq& \frac{L}{NK}\sum_{i,k}\mathbb{E}\left\|\boldsymbol{\theta}_i^{0,k} - \boldsymbol{\theta}^0\right\| + \frac{3\sigma}{\sqrt{SK}} \\
\leq& \frac{1}{2}\eta KL + \frac{3\sigma}{\sqrt{SK}}.
\end{aligned} \tag{A16}$$

Then, we have

$$\left\|\boldsymbol{w}^t\right\| \leq \frac{L}{SK}\sum_{i\in\mathcal{S}_t,k}\mathbb{E}\left\|\boldsymbol{\theta}_i^{t,k} - \boldsymbol{\theta}^t\right\| \leq \frac{1}{2}\eta KL. \tag{A17}$$

Additionally, since $\mathbb{E}[\widetilde{\boldsymbol{u}}^t|\mathcal{F}^t] = \mathbf{0}$, then, for any $0 \leq t_1 < t_2 \leq T-1$, we have

$$\mathbb{E}\left\langle\widetilde{\boldsymbol{u}}^{t_1}, \widetilde{\boldsymbol{u}}^{t_2}\right\rangle = \mathbb{E}\left\langle\widetilde{\boldsymbol{u}}^{t_1}, \mathbb{E}[\widetilde{\boldsymbol{u}}^{t_2}|\mathcal{F}^{t_2}]\right\rangle = 0.$$

From Lemma 2, for any t, we have

$$\begin{aligned}
\mathbb{E}\left\|\widetilde{\boldsymbol{u}}^t\right\|^2 \leq& \mathbb{E}\left\|\frac{1}{NK}\sum_{i,k}\left(\nabla F\left(\boldsymbol{\theta}^{t-1}; \boldsymbol{\xi}_i^{t,k}\right) - \nabla F\left(\boldsymbol{\theta}^t; \boldsymbol{\xi}_i^{t,k}\right)\right) + \nabla f\left(\boldsymbol{\theta}^t\right) - \nabla f\left(\boldsymbol{\theta}^{t-1}\right)\right\|^2 \\
&+ \frac{1}{SN}\sum_{i=1}^N\mathbb{E}\left\|\frac{1}{K}\sum_k\left(\nabla F\left(\boldsymbol{\theta}^{t-1}; \boldsymbol{\xi}_i^{t,k}\right) - \nabla F\left(\boldsymbol{\theta}^t; \boldsymbol{\xi}_i^{t,k}\right)\right) + \nabla f\left(\boldsymbol{\theta}^t\right) - \nabla f\left(\boldsymbol{\theta}^{t-1}\right)\right\|^2 \\
\leq& \frac{L^2}{NK}\left\|\boldsymbol{\theta}^t - \boldsymbol{\theta}^{t-1}\right\|^2 + \frac{L^2}{SK}\left\|\boldsymbol{\theta}^t - \boldsymbol{\theta}^{t-1}\right\|^2 \\
\leq& \frac{2\gamma^2L^2}{SK}.
\end{aligned}$$

Then, we have

$$\mathbb{E}\left\|\sum_{\tau=1}^t\widetilde{\boldsymbol{u}}^\tau(1-\beta)^{t+1-\tau}\right\|^2 = \sum_{\tau=1}^t\mathbb{E}\|\widetilde{\boldsymbol{u}}^\tau\|^2(1-\beta)^{t+1-\tau} \leq \frac{2\gamma^2L^2}{SK\beta}. \tag{A18}$$

Similarly, since $\mathbb{E}[\widetilde{\boldsymbol{v}}^t|\mathcal{F}^t] = \mathbf{0}$, for any $0 \leq t_1 < t_2 \leq T-1$, we have

$$\mathbb{E}\left\langle\widetilde{\boldsymbol{v}}^{t_1}, \widetilde{\boldsymbol{v}}^{t_2}\right\rangle = \mathbb{E}\left\langle\widetilde{\boldsymbol{v}}^{t_1}, \mathbb{E}[\widetilde{\boldsymbol{v}}^{t_2}|\mathcal{F}^{t_2}]\right\rangle = 0.$$

From Lemma 2, for any t, we have

$$\begin{aligned}
\mathbb{E}\|\widetilde{\boldsymbol{v}}^t\|^2 \leq& \mathbb{E}\left\|\nabla f\left(\boldsymbol{\theta}^t\right) - \frac{1}{NK}\sum_{i,k}\nabla F\left(\boldsymbol{\theta}^t; \boldsymbol{\xi}_i^{t,k}\right)\right\|^2 + \frac{1}{SN}\sum_{i=1}^N\left\|\frac{1}{K}\sum_k\nabla F\left(\boldsymbol{\theta}^t; \boldsymbol{\xi}_i^{t,k}\right) - \boldsymbol{c}_i^{t-1}\right\|^2 \\
\leq& \frac{\sigma^2}{NK} + \frac{1}{SN}\sum_{i=1}^N\left\|\frac{1}{K}\sum_k\nabla F\left(\boldsymbol{\theta}^t; \boldsymbol{\xi}_i^{t,k}\right) \mp \nabla f_i\left(\boldsymbol{\theta}^t\right) \mp \nabla f_i\left(\boldsymbol{\theta}^{t-1}\right) - \boldsymbol{c}_i^{t-1}\right\|^2 \\
\leq& \frac{\sigma^2}{NK} + \frac{3\sigma^2}{SK} + \frac{3}{S}\gamma^2L^2 + \frac{3}{S}\frac{1}{N}\sum_{i=1}^N\boldsymbol{\phi}_i^{t-1}.
\end{aligned}$$

By (A10), $\phi_i^{t-1} \leq \frac{6\sigma^2}{K} + 2\eta^2 K^2 L^2 + \frac{4N^2}{S^2}\gamma^2 L^2$. Then, we have

$$\mathbb{E}\|\widetilde{\boldsymbol{v}}^t\|^2 \leq \frac{22\sigma^2}{SK} + \frac{3\gamma^2 L^2}{S}\left(1 + \frac{4N^2}{S^2}\right) + \frac{6}{S}\eta^2 K^2 L^2.$$

$$\begin{aligned}\mathbb{E}\left\|\sum_{\tau=1}^{t}\beta\widetilde{\boldsymbol{v}}^\tau(1-\beta)^{t-\tau}\right\|^2 &\leq \beta^2\sum_{\tau=1}^{t}\mathbb{E}\|\widetilde{\boldsymbol{v}}^\tau\|^2(1-\beta)^{t+1-\tau} \\ &\leq \frac{22\beta\sigma^2}{SK} + \frac{3\beta\gamma^2 L^2}{S}\left(1 + \frac{4N^2}{S^2}\right) + \frac{6\beta}{S}\eta^2 K^2 L^2. \end{aligned} \tag{A19}$$

Plugging (A16), (A17), (A18), and (A19) into (A15) yields

$$\begin{aligned}\mathbb{E}\|\mathcal{E}^t\| \leq &(1-\beta)^t\left(\frac{1}{2}\eta KL + \frac{3\sigma}{\sqrt{SK}}\right) + \frac{\eta KL}{2\beta} + \gamma L\sqrt{\frac{2}{SK\beta}} + \sigma\sqrt{\frac{22\beta}{SK}} \\ &+ \gamma L\sqrt{\frac{3\beta}{S}\left(1 + \frac{4N^2}{S^2}\right)} + \eta KL\sqrt{\frac{6\beta}{S}}.\end{aligned}$$

Summing the above inequality over t yields

$$\begin{aligned}\frac{1}{T}\sum_{t=0}^{T-1}\mathbb{E}\|\mathcal{E}^t\| \leq &\frac{1}{\beta T}\left(\frac{1}{2}\eta KL + \frac{3\sigma}{\sqrt{SK}}\right) + \frac{\eta KL}{2\beta} + \gamma L\sqrt{\frac{2}{SK\beta}} + \sigma\sqrt{\frac{22\beta}{SK}} \\ &+ \gamma L\sqrt{\frac{3\beta}{S}\left(1 + \frac{4N^2}{S^2}\right)} + \eta KL\sqrt{\frac{6\beta}{S}}.\end{aligned}$$

C.2 Proof of Lemma 7

With variance reduction, we have $\boldsymbol{g}_i^{t,k} = \nabla F\left(\boldsymbol{\theta}_i^{t,k}; \boldsymbol{\xi}_i^{t,k}\right) - \beta\left(\boldsymbol{c}_i^{t-1} - \boldsymbol{c}^{t-1}\right) + (1-\beta)\left(\boldsymbol{g}^{t-1} - \nabla F\left(\boldsymbol{\theta}^{t-1}; \boldsymbol{\xi}_i^{t,k}\right)\right)$. Since $\boldsymbol{g}^t = \frac{1}{SK}\sum_{i\in\mathcal{S}_t,k}\boldsymbol{g}_i^{t,k}$, we have

$$\begin{aligned}&\mathbb{E}\left[\frac{1}{SK}\sum_{i\in\mathcal{S}_t}\left\|\boldsymbol{g}_i^{t,k} - \boldsymbol{g}^t\right\|\right] \\ &\leq \frac{2}{NK}\sum_{i,k}\mathbb{E}\left\|\nabla F\left(\boldsymbol{\theta}_i^{t,k}; \boldsymbol{\xi}_i^{t,k}\right) - \beta\boldsymbol{c}_i^{t-1} - (1-\beta)\nabla F\left(\boldsymbol{\theta}^{t-1}; \boldsymbol{\xi}_i^{t,k}\right)\right\| \\ &\leq \frac{2}{NK}\sum_{i,k}\left(\beta\mathbb{E}\left\|\nabla F\left(\boldsymbol{\theta}_i^{t,k}; \boldsymbol{\xi}_i^{t,k}\right) - \boldsymbol{c}_i^{t-1}\right\| + (1-\beta)\mathbb{E}\left\|\nabla F\left(\boldsymbol{\theta}_i^{t,k}; \boldsymbol{\xi}_i^{t,k}\right) - \nabla F\left(\boldsymbol{\theta}^{t-1}; \boldsymbol{\xi}_i^{t,k}\right)\right\|\right) \\ &\leq \frac{2\beta}{NK}\sum_{i,k}\mathbb{E}\left\|\nabla F\left(\boldsymbol{\theta}_i^{t,k}; \boldsymbol{\xi}_i^{t,k}\right) - \boldsymbol{c}_i^{t-1}\right\| + 2L(1-\beta)\left(\frac{1}{NK}\sum_{i,k}\mathbb{E}\left\|\boldsymbol{\theta}_i^{t,k} - \boldsymbol{\theta}^t\right\| + \mathbb{E}\left\|\boldsymbol{\theta}^t - \boldsymbol{\theta}^{t-1}\right\|\right) \\ &\leq \frac{2\beta}{NK}\sum_{i,k}\mathbb{E}\left\|\nabla F\left(\boldsymbol{\theta}_i^{t,k}; \boldsymbol{\xi}_i^{t,k}\right) - \boldsymbol{c}_i^{t-1}\right\| + \eta KL + 2\gamma L.\end{aligned}$$

From Section B.2, we know that

$$\begin{aligned}\frac{2\beta}{NK}\sum_{i,k}\mathbb{E}\left\|\nabla F\left(\boldsymbol{\theta}_i^{t,k}; \boldsymbol{\xi}_i^{t,k}\right) - \boldsymbol{c}_i^{t-1}\right\| \leq &2\beta\left(\left(1 + \frac{2}{\sqrt{K}}\right)\sigma + 2\eta KL + \left(1 + \frac{2N}{S}\right)\gamma L\right) \\ &+ 2\beta\left(\frac{\sqrt{2}\sigma}{\sqrt{K}} + \sqrt{\frac{2S}{3N}}\eta KL\right)\left(1 - \frac{S}{4N}\right)^{t-1}.\end{aligned}$$

Then, we have

$$\mathbb{E}\left[\frac{1}{SK}\sum_{i\in\mathcal{S}_t}\left\|\boldsymbol{g}_i^{t,k}-\boldsymbol{g}^t\right\|\right] \leq 2\beta\left(\left(1+\frac{2}{\sqrt{K}}\right)\sigma+2\eta KL+\left(1+\frac{2N}{S}\right)\gamma L\right) + 2\beta\left(\frac{\sqrt{2}\sigma}{\sqrt{K}}+\sqrt{\frac{2S}{3N}}\eta KL\right)\left(1-\frac{S}{4N}\right)^{t-1}+\eta KL+2\gamma L.$$

Summing the above inequality over t, we have

$$\frac{1}{SKT}\sum_{t=1}^{T}\mathbb{E}\left[\sum_{i\in\mathcal{S}_t,k}\left\|\boldsymbol{g}_i^{t,k}-\boldsymbol{g}^t\right\|\right] \leq 2\beta\left(\left(1+\frac{2}{\sqrt{K}}\right)\sigma+2\eta KL+\left(1+\frac{2N}{S}\right)\gamma L\right) + \frac{8N\beta}{ST}\left(\frac{\sqrt{2}\sigma}{\sqrt{K}}+\sqrt{\frac{2S}{3N}}\eta KL\right)+\eta KL+2\gamma L.$$

D Additional Numerical Results

In this section, we provide detailed simulation settings and present the results for the textual sentiment analysis task.

Datasets. 1) **Image Dataset:** The EMNIST dataset (Cohen et al., 2017) extends the MNIST dataset, featuring images of handwritten letters and digits. It includes both uppercase and lowercase English letters as well as digits from 0 to 9. 2) **Natural Language Dataset:** The IMDB dataset (Maas et al., 2011) contains movie reviews sourced from the Internet Movie Database, with each review labeled as either positive or negative sentiment.

Experimental Settings: Our evaluation encompasses both image classification and textual sentiment analysis tasks. For image classification, we employ a convolutional neural network (CNN) with three convolutional layers and two fully connected layers for the EMNIST dataset, and a ResNet-18 architecture for CIFAR-10. The sentiment analysis task utilizes a Long Short-Term Memory (LSTM) model on the IMDB dataset. The experimental framework involves 100 distributed clients, with 10 clients participating randomly in each training round. We investigate both independent and identically distributed (i.i.d.) and non-i.i.d. data distributions. For i.i.d. scenarios, we implement uniform random data distribution across clients. To simulate realistic heterogeneity in non-i.i.d. settings, we apply different statistical distributions: a Dirichlet distribution Dir(1) for EMNIST, Dir(0.5) for CIFAR-10, and a Beta distribution Beta(2,5) for IMDB. All hyperparameters, including learning rates, are optimized through comprehensive grid search.

D.1 Simulations on CIFAR-10 Dataset

Figure 3 presents the comparative analysis of test accuracy across different algorithms on the CIFAR-10 dataset, with subfigures 3a and 3b illustrating the performance under i.i.d. and non-i.i.d. data distributions, respectively. The observed patterns align with those demonstrated in Figure 1. Our proposed algorithms demonstrate superior performance compared to existing methods, including FedAvg, SCAFFOLD, and SCAFFOLD-M, both in terms of convergence rate and final test accuracy. Under non-i.i.d. conditions, while all algorithms exhibit increased performance volatility and reduced accuracy, the relative performance hierarchy remains consistent with the i.i.d. scenario, as shown in subfigure 6b.

Figure 4 illustrates the evolution of gradient norm $|\nabla f(\boldsymbol{\theta}_t)|$ for various algorithms on the CIFAR-10 dataset under both i.i.d. and non-i.i.d. data distributions. The results demonstrate that momentum-enhanced methods, specifically our proposed algorithm and SCAFFOLD-M, achieve more rapid gradient norm reduction compared to their non-momentum counterparts.

We further carry out the ablation study by isolating the effects of momentum and gradient normalization in Figure 5. The results demonstrate that incorporating SCAFFOLD with normalized gradient leads to degraded performance due to the loss of gradient magnitude information. Therefore, the momentum is essential in our algorithm design to maintain the descent direction by effectively aggregating gradients across clients and iterations.

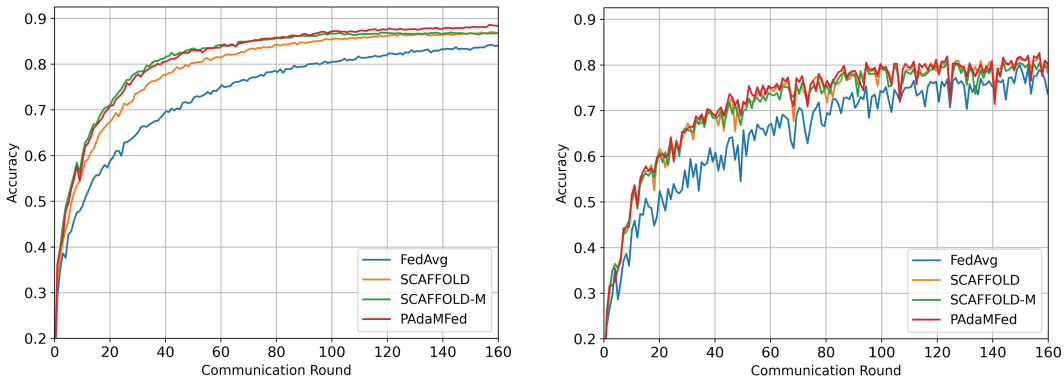

(a) i.i.d (b) non-i.i.d

Figure 3: Test accuracy versus the number of communication rounds on the CIFAR-10 dataset.

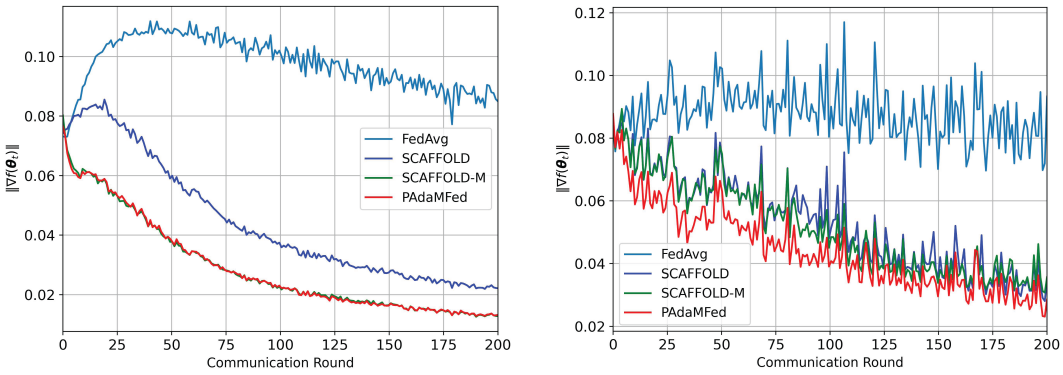

(a) i.i.d (b) non-i.i.d

Figure 4: Gradient norm versus the number of communication rounds on the CIFAR-10 dataset.

D.2 Simulations on IMDB Dataset

Figure 6 shows the test accuracy of various algorithms versus the number of communication rounds on the IMDB dataset, with subfigure 6a representing i.i.d. data and subfigure 1b depicting non-i.i.d. data. In general, the results are similar to those in Figure 1 and Figure 3, but with smoother curves. This may be attributed to the fact that the text sentiment analysis task, which is a binary classification problem (positive or negative), is simpler than the image classification task. First, we observe that our algorithms significantly outperform all the compared algorithms, including FedAvg, SCAFFOLD, and SCAFFOLD-M, in both convergence speed and test accuracy. Second, due to the judicious combination of adaptive stepsizes, PAdaMFed surpasses its counterpart, SCAFFOLD-M, which only uses momentum in its local updates. Additionally, variance reduction improves PAdaMFed's performance through more efficient sample utilization. Finally, our algorithm's superiority is even more pronounced on non-i.i.d. data, as demonstrated in subfigure 6b.

Figure 7 compares test accuracy against the learning rate on the IMDB dataset. We only compare our algorithm with SCAFFOLD-M, as it performed the best among the comparison baselines in the classification task. We observe that across the entire stepsize range, our algorithm consistently outperforms SCAFFOLD-M in test accuracy for both i.i.d. and non-i.i.d. data settings. However, compared to the image classification task, the performance margin of our algorithm is less pronounced, likely due to the simplicity of the binary classification task in text sentiment analysis. Additionally, because of this simplicity, the performance of both algorithms in the non-i.i.d. setting is comparable to that in the i.i.d. case, which contrasts with the image classification task.

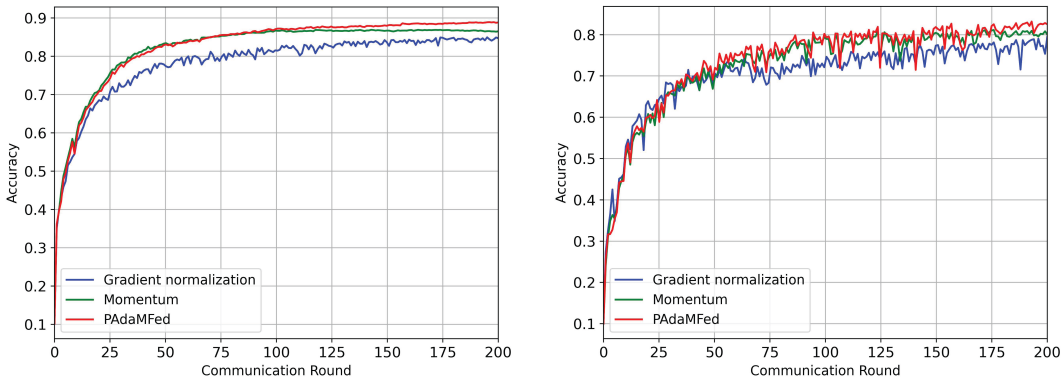

(a) i.i.d (b) non-i.i.d

Figure 5: Ablation study versus the number of communication rounds on the CIFAR-10 dataset.

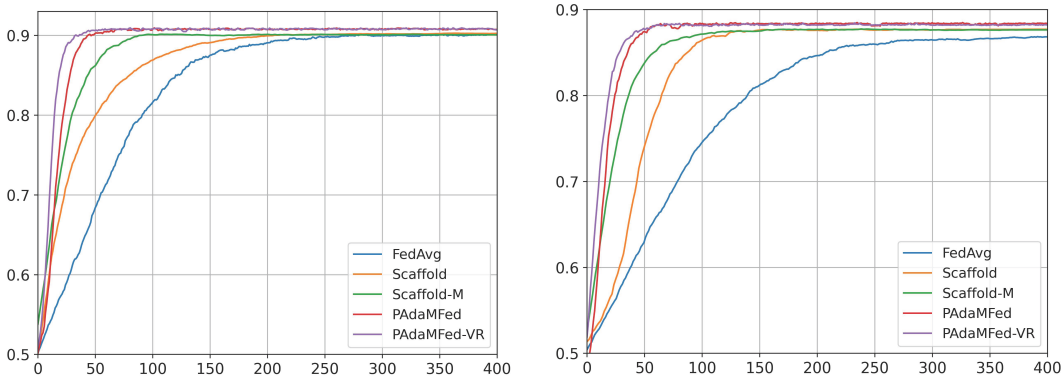

(a) i.i.d (b) non-i.i.d

Figure 6: Test accuracy versus the number of communication rounds on the IMDB dataset.

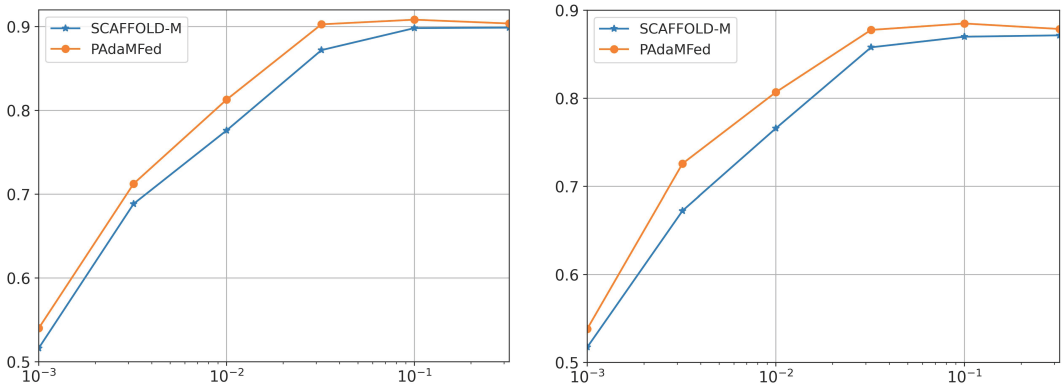

(a) i.i.d (b) non-i.i.d

Figure 7: Test accuracy versus learning rate on the IMDB dataset.